Versão do arquivo anexado / Version of attached file:

Versão do Editor / Published Version

Mais informações no site da editora / Further information on publisher's website:

https://www.sciencedirect.com/science/article/pii/S2589004219303827

DOI: 10.1016/j.isci.2019.10.003

Direitos autorais / Publisher's copyright statement:

Article

Structural Basis of Colchicine-Site targeting Acylhydrazones active against Multidrug-Resistant Acute Lymphoblastic Leukemia
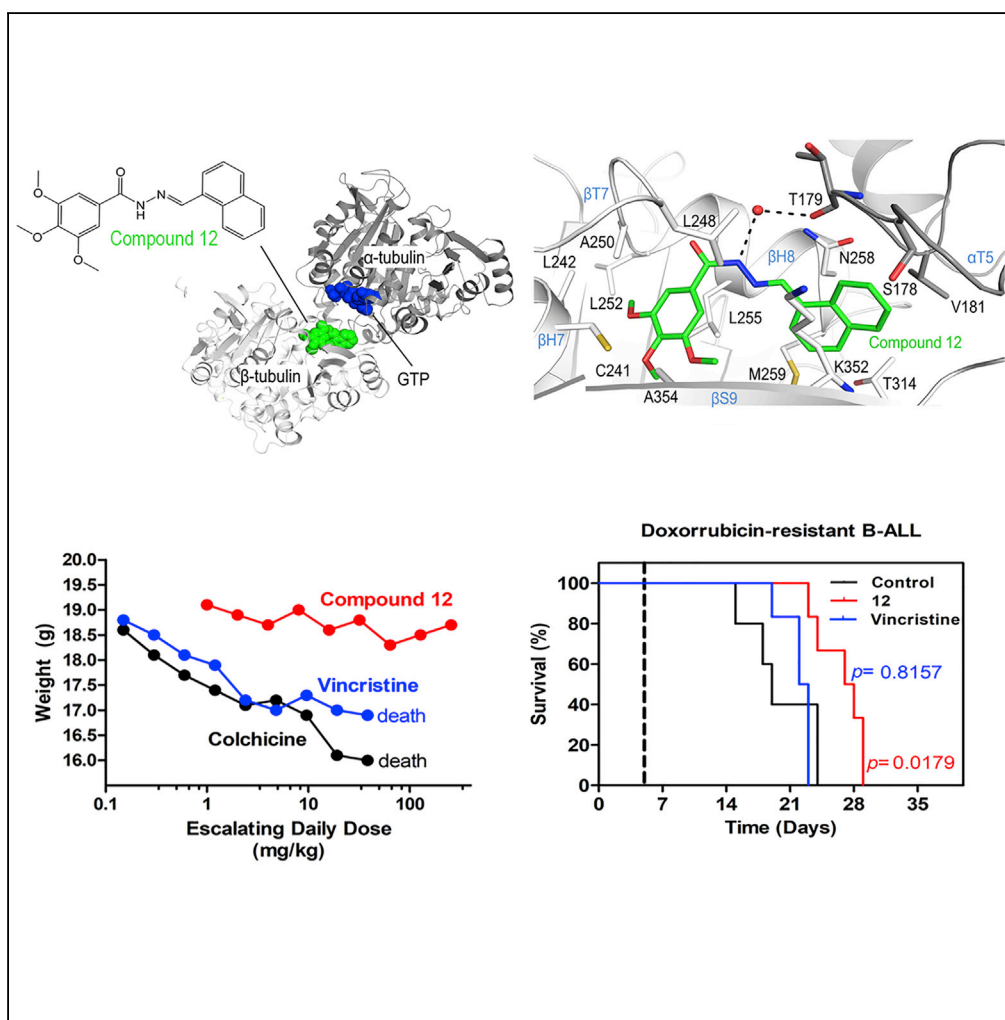
Nathália Moreno Cury, Tobias Mühlethaler, Angelo Brunelli Albertoni Laranjeira, ..., Michel Olivier Steinmetz, José Fernando Díaz, José Andrés Yunes

andres@boldrini.org.br

HIGHLIGHTS

3,4,5-trimethoxy-*N*-acylhydrazones bind to the colchicine site of tubulin

12 forms a single H-bond with αThr179 and causes steric hindrance of tubulin βT7 loop

3,4,5-trimethoxy-*N*-acylhydrazones feature low toxicity

12 shows therapeutic effect against multidrug-resistant acute lymphoblastic leukemia

DATA AND CODE AVAILABILITY

6F7C

iScience

CellPress

Article

Structural Basis of Colchicine-Site targeting Acylhydrazones active against Multidrug-Resistant Acute Lymphoblastic Leukemia

Nathália Moreno Cury,[1,2] Tobias Mühlethaler,[3] Angelo Brunelli Albertoni Laranjeira,[1] Rafael Renatino Canevarolo,[1] Priscila Pini Zenatti,[1] Daniel Lucena-Agell,[4] Isabel Barasoain,[4] Chunhua Song,[5] Dongxiao Sun,[5] Sinisa Dovat,[5] Rosendo Augusto Yunes,[6] Andrea Enrico Prota,[3] Michel Olivier Steinmetz,[3,7] José Fernando Díaz,[4] and José Andrés Yunes[1,8,9,*]

SUMMARY

Tubulin is one of the best validated anti-cancer targets, but most anti-tubulin agents have unfavorable therapeutic indexes. Here, we characterized the tubulin-binding activity, the mechanism of action, and the *in vivo* anti-leukemia efficacy of three 3,4,5-trimethoxy-*N*-acylhydrazones. We show that all compounds target the colchicine-binding site of tubulin and that none is a substrate of ABC transporters. The crystal structure of the tubulin-bound *N*-(1′-naphthyl)-3,4,5-trimethoxybenzohydrazide (12) revealed steric hindrance on the T7 loop movement of β-tubulin, thereby rendering tubulin assembly incompetent. Using dose escalation and short-term repeated dose studies, we further report that this compound class is well tolerated to >100 mg/kg in mice. We finally observed that intraperitoneally administered compound 12 significantly prolonged the overall survival of mice transplanted with both sensitive and multidrug-resistant acute lymphoblastic leukemia (ALL) cells. Taken together, this work describes promising colchicine-site-targeting tubulin inhibitors featuring favorable therapeutic effects against ALL and multidrug-resistant cells.

INTRODUCTION

Despite the success already achieved in the treatment of children with acute lymphoblastic leukemia (ALL), relapse still occurs in around 20% of patients (Steinherz et al., 1996; Stock et al., 2013). The overall survival rate for relapsed childhood ALL is approximately 40%–60% despite intensive chemotherapy and allogeneic stem cell transplantation (Oskarsson et al., 2015; Roy et al., 2005), highlighting the need for new drugs or new drug formulations. Recent clinical trials in adults (reviewed in Soosay Raj et al., 2013) and children (Shah et al., 2016) with relapsed or refractory ALL have shown promising results with the use of liposomal vincristine. Vincristine has been in clinical use for decades and is one of the main components of every ALL protocol. Liposomal vincristine allowed the use of higher and more frequent doses of this anti-tubulin agent by circumventing its neurotoxic effects, which are likely caused by perturbations of microtubule functions that are essential for axonal transport in neurons (Shah et al., 2016; Soosay Raj et al., 2013).

Tubulin is one of the best validated targets for cancer therapy. There are dozens of new anti-tubulin agents in clinical or late preclinical development, pursuing better therapeutic indexes, i.e., a better trade-off between efficacy and toxicity (Field et al., 2015; Liu et al., 2014; Wood et al., 2001). In this context, our group has designed and tested a series of 3,4,5-trimethoxy-*N*-acylhydrazones some of which exhibited strong anti-microtubule and anti-leukemia activities, *in vitro* and *in vivo*, while showing modest toxicity toward normal proliferating T cells (Salum et al., 2015). In this study, we highlight the biochemical and biological properties of three 3,4,5-trimethoxy-*N*-acylhydrazones: compounds **7**, **12**, and **21**, which showed the best *in vitro* anti-leukemic effects in our previous study (Salum et al., 2015).

RESULTS

Compounds 7, 12, and 21 Bind to the Colchicine-Binding Site of Tubulin and Inhibit Microtubule Assembly

Our previously reported computational docking efforts propose that *N*-acylhydrazones could adopt an appropriate stereochemistry in the colchicine-binding site of tubulin (Salum et al., 2015). To test the
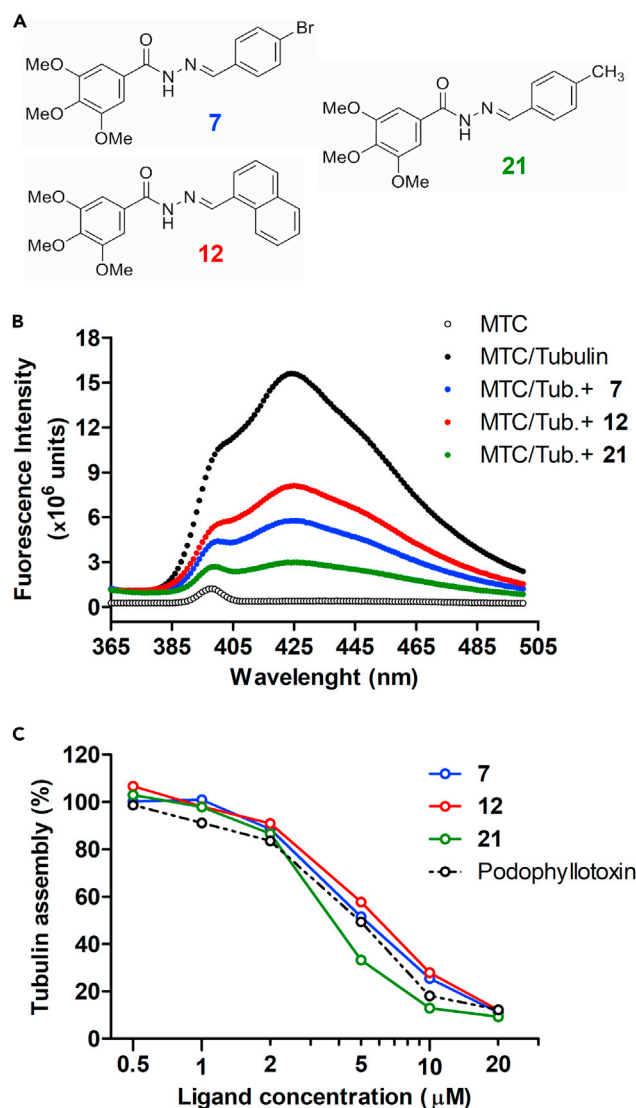
Figure 1. Compounds 7, 12, and 21 Are Colchicine-Binding Site Tubulin Inhibitors

(A) Derivatives from *N*-acylhydrazones with the best *in vitro* anti-leukemic effects in Salum et al. (2015).

(B) Displacement of MTC from the colchicine-binding site by *N*-acylhydrazones. Fluorescence intensity of MTC bound to tubulin after addition of 10 μM compounds **7**, **12**, and **21**. Each curve represents the mean of three independent experiments. See also Figure S2.

(C) Inhibition of tubulin assembly by compounds **7**, **12**, **21**, and podophyllotoxin after 85 min of incubation. Absorbance spectra of 25 μM tubulin in the presence of different concentrations (0.5–20 μM) of the three compounds studied or DMSO (vehicle) was monitored over time by turbidity.

See also Figure S3.

interaction of compounds **7**, **12**, and **21** (Figure 1A) with tubulin, we assessed the UV absorbance spectrum of these compounds (Figure S1) followed by their ability to displace 2-methoxy-5-(2′,3′,4′-trimethoxy)-2,4,6-cycloheptatrien-1-one (MTC), a reversible tubulin ligand targeting the colchicine-binding site (Fitzgerald, 1976).

Compounds **7**, **12**, and **21** were capable of displacing the MTC probe, confirming their binding to the colchicine pocket of tubulin (Figure 1B). Calculation of binding constants (Figure S2) revealed that compound **21** binds tubulin with a 10 times higher affinity (binding constant of 5.0×10^7 M^{-1}) than compounds **7** (3.3×10^6 M^{-1}) and **12** (1.26×10^6 M^{-1}). For comparison, podophyllotoxin's binding constant for tubulin, in the same assay, was reported to be 1.85×10^7 M^{-1} (Antúnez-Mojica et al., 2016).

In the tubulin polymerization assay, which included podophyllotoxin as a positive control, all three compounds were effective in inhibiting tubulin polymerization (Figure 1C). Inhibition of tubulin assembly by these compounds over time is shown in Figure S3. We further investigated the effects of these compounds in cellular tubulin depolymerization assays using the A-549 cell line. Microtubule network depolymerization occurred at 200 nM for compounds **12** and **21**, at 300 nM for compound **7**, and at 100 nM for colchicine, which was included as positive control (Figure 2A). Compound **21** was slightly more potent than the other two compounds, because cells could be seen arrested in prometaphase and DNA was arranged in a ball of condensed chromosomes with no microtubules, which is a type IV spindle. On the other hand, in mitotic spindles seen in cells treated with compounds **7** and **12** the chromosomes were arranged in a ball enclosing several star-shaped aggregates of microtubules characteristic of type III spindles (Jordan et al., 1992). In all cases, mitotic arrest was accompanied by net microtubule depolymerization (Figure 2A).

Although compounds **7** and **12** had similar effects in the MTC displacement and tubulin depolymerization assays, compound **12** was slightly more potent than compound **7** in promoting cellular microtubule depolymerization (Figure 2A), suggesting that compound **12** may have a better cellular bioavailability. Thus, the next step was to investigate the cellular uptake of compounds **7**, **12**, and **21**, after 30 min, 6 h, and 12 h of incubation with each compound at a concentration (100 nM) that is close to their IC_{50} in cytotoxic assays. As expected, mass spectrometric analyses of total cellular extracts showed a significant lower cellular uptake of compound **7**. Compound **12** had higher uptake after 30 min of treatment. However, its level decreased after 6 and 12 h, whereas the amount of compound **21** increased with time (Figure 2B). Whether compound **12** is subjected to cellular metabolization remains to be investigated.

Compounds 7, 12, and 21 Are Not Substrates of ATP-Binding Cassette Transporters

Overexpression of ATP-binding cassette (ABC) transporters is involved in the cellular resistance to vinca alkaloids and anti-cancer drugs in general, constituting one of the main causes of failure in cancer therapy (El-Awady et al., 2017). To evaluate if compounds **7**, **12**, and **21** were substrates of ABC transporter proteins, cell viability assays were performed using four pairs of cell lines, each pair including a parental sensitive cell line and its resistant derivative, known to overexpress ABC transporters. All resistant cells displayed a typical multidrug resistance (MDR) phenotype, as evaluated by the calcein exclusion assay (Figure S4). Compounds **7**, **12**, and **21** showed similar IC_{50} values (Table 1) and cell-cycle arrest potency (Figure S5) for both sensitive and resistant cell lines, indicating that these compounds are not good substrates of ABC transporter proteins, which was not the case for colchicine, vinblastine, and vincristine. However, a modest 4- to 9-fold increased resistance to the acylhydrazone compounds was observed for the colchicine-resistant mouse 3T3 embryonic fibroblastoid cell line. Considering the three pair of neoplastic cell lines, compound **12** showed the lowest IC_{50} for all six cell lines, followed by compounds **21** and **7**, respectively (Table 1).

Cell-Cycle Arrest, DNA Damage, and Apoptosis Caused by Acylhydrazone Compounds

We choose compound **12**, which presented the best *in vitro* cytotoxic results, as our leading compound for further mechanistic investigations. Increased *in vitro* proliferation of primary ALL cells was found to correlate with increased sensitivity to some chemotherapeutic drugs, including vincristine (Kaaijk et al., 2003). As shown in Figure 3, we found no correlation (p = 0.1821) between the doubling time and *in vitro* resistance (IC_{50}) to compound **12** on a series of different precursor B cell ALL and T cell ALL cell lines (Table S1). To investigate how compound **12** leads to cell death, the pre-B ALL leukemia cell line RS4;11 was treated with compound **12** for 18 h and then labeled with bromodeoxyuridine (BrdU) and stained with antibodies against H2AX and PARP. Treatment with compound **12** resulted in a population of cells with DNA content in between G1 and G2, suggesting the occurrence of unequal division (Figure 4). DNA damage (H2AX) and apoptosis (PARP) occurred both at the G1 and G2 phases of the cell cycle. These results suggest that cells treated with compound **12** face cell death both as a consequence of mitotic arrest (in G2/M) and after unequal division; however, we cannot exclude the possibility of mitotic slippage followed by post-slippage cell death. As unequal division could lead to the continuous cycling of some genomically unstable cells, and the risk of secondary tumors, we investigated the generation of micronuclei. As shown in Table 2 micronuclei induction by compound **12** was comparable to that by colchicine and significantly lower than that by vincristine.

Crystal Structure of the Tubulin Compound 12 Complex

To elucidate the tubulin-binding mode of compound **12**, we solved its structure in complex with tubulin by X-ray crystallography. To obtain crystals of tubulin, we complexed two α/β-tubulin heterodimers from
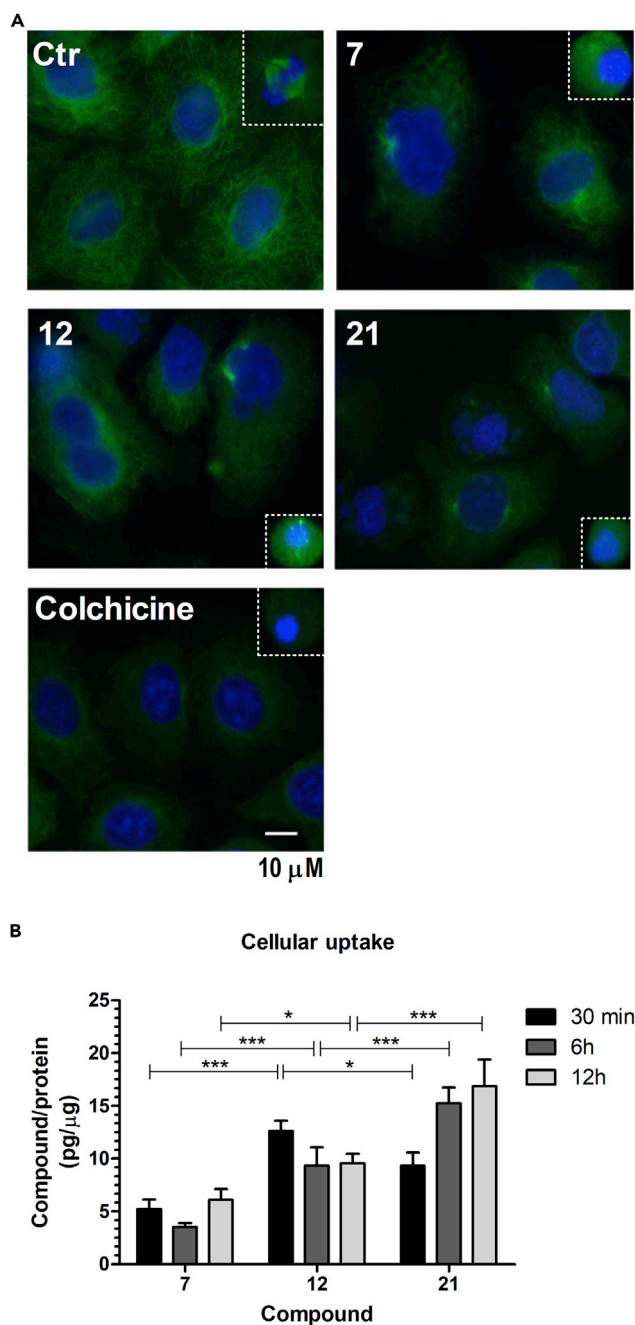
Figure 2. Effects of Compounds 7, 12, and 21 on Microtubule Cytoskeleton and Their Cellular Uptake

(A) Effects of compounds **7**, **12**, and **21** on the cellular microtubule network of A-549 cells. A-549 cells were incubated for 20 h with DMSO (control, Ctr), 300 nM of **7**, 200 nM of **12**, 200 nM of **21**, or 100 nM of colchicine. Anti-α-tubulin antibodies and Hoechst 33342 were used to stain microtubules (green) and DNA (blue), respectively. Mitotic spindles from the same preparation are shown in the right corner of each picture.

(B) Amount of compounds **7**, **12**, and **21** in total cellular lysates of CEM leukemia cells after 0.5, 6, or 12 h of treatment with 100 nM of the corresponding compound. The amount of each compound was normalized by the amount of protein from the same sample. Each bar represents the mean $\pm$ SD of three biological replicates. Data were analyzed by the two-way ANOVA followed by Bonferroni's post-test for mean comparisons (*$p < 0.05$; **$p < 0.01$; ***$p < 0.001$).

Compounds versus Cell Lines	7	12	21	Colchicine	Vinblastine	Vincristine
A2780	144 ± 6	48 ± 1	82 ± 14	23 ± 5	0.5 ± 0.1	3 ± 0.4
A2780/AD	101 ± 11.1	20.6 ± 2.0	55.9 ± 1.4	270 ± 49	29 ± 5	457 ± 131
Ratio[a]	0.7	0.4	0.7	11.7	57.3	154.6
KB	103 ± 1.3	19.7 ± 5.6	43.2 ± 11	18.6 ± 0.7	0.23	0.7
KB/VB	107 ± 12.1	20.3 ± 2.4	46.9 ± 10	724 ± 228	85.9 ± 3.3	1130 ± 100
Ratio	1.04	1.03	1.09	38.9	374.3	1608
CEM	116 ± 27.6	31.4 ± 8	54 ± 0.7	14.5 ± 0.3	0.6	0.7 ± 0.2
CEM/VCR	122 ± 25	32 ± 11	50 ± 6	281 ± 5	128 ± 3	1700 ± 131
Ratio	1.05	1.02	0.93	19.42	213.65	2322.52
NIH3T3	65.7 ± 4.4	13.2 ± 4.3	109 ± 15	30 ± 3.5	1.02 ± 0.02	2.8 ± 0.7
NIH-MDR-G185	268 ± 50	95.8 ± 22	984 ± 302	783 ± 64.7	33.2 ± 0.95	898 ± 111
Ratio	4.08	7.25	9.02	26.1	32.5	320.7

Table 1. Cytotoxicity Data (IC$_{50}$ ± SD, nM) for Compounds 7, 12, 21, Colchicine, Vinblastine, and Vincristine against Human Neoplastic Cell Lines

Cytotoxicity results are expressed as IC$_{50}$ values, the compound concentrations producing 50% cell growth inhibition, and represent the mean ± SD of three to five independent experiments.

[a]Determined by dividing the resistant cell line IC$_{50}$ mean by the sensitive cell line IC$_{50}$ mean.

bovine brain with rat stathmin-like protein RB3 and chicken tubulin tyrosine ligase (the complex is denoted T$_2$R-TTL) (Prota et al., 2013a, 2013b). Subsequently, the compound was soaked into the T$_2$R-TTL crystals, and we were able to obtain X-ray diffraction data to 2.0 Å resolution (Table S2). We found that only the colchicine site of the α1β1-tubulin was occupied with compound 12 (Figures 5A and S6). Superimposing the T$_2$R-TTL-compound 12 complex structure with the unliganded T$_2$R-TTL structure (PDB: 4IHJ) showed no major conformational changes upon ligand binding (root-mean-square deviation of 0.33 Å over 1,864 Cα-atoms).

The trimethoxyphenyl moiety of compound 12 fits in a predominantly hydrophobic pocket shaped by the side chains of βTyr202, βCys241, βLeu242, βLeu248, βAla250, βLeu252, βLeu255, βAla316, βIle318, βAla354, and βIle378 (Figure 5B). A second predominantly hydrophobic pocket is shaped by βAsn258, βMet259, βThr314, βAla316, βLys352, αSer178, and αVal181 into which the naphthalene moiety of compound 12 is inserted. The structure also reveals a water-mediated hydrogen bond between the nitrogen of the acylhydrazone linker of compound 12 and the backbone of αThr179. A previous docking study (Salum et al., 2015) proposed three additional hydrogen bonds. The first one is between the oxygen of the 3′-methoxy of compound 12 and the side chain of βCys241; our tubulin compound 12 crystal structure shows a distance between the two atoms of 3.9 Å, which seems too long to allow for the permanent formation of a stable hydrogen bond. The other two hydrogen bonds were predicted to be formed between the carbonyl group of compound 12 and the main chains of βAsp251 and βLeu255. Our tubulin compound 12 crystal structure reveals distances of 3.6 and 4.3 Å, respectively, which are on the higher side to establish stable hydrogen bonds. In conclusion, our analysis reveals that compound 12 establishes a single hydrogen bond with tubulin.

To elucidate the mode of action of compound 12 on tubulin, we superimposed several T$_2$R-TTL crystal structures. First, we compared the tubulin-compound 12 structure with the apo structure of tubulin (PDB: 4IHJ). The major difference observed concerns the βT7 loop, which is flipped outward upon binding of the ligand (Figure 5C). Second, we superimposed the binding mode of compound 12 onto the tubulin-colchicine complex structure (PDB: 4O2B; Figure 5D). This analysis shows a large overlap of the two ligands with only a minor shift of the αT5 loop due to the differing sizes of the two ligands. The βT7 loop is flipped outward to nearly the same position for both compound 12 and colchicine. These observations indicate that compound 12, like colchicine, causes steric hindrance on the βT7 loop movement, thus locking tubulin in an assembly-incompetent conformation.
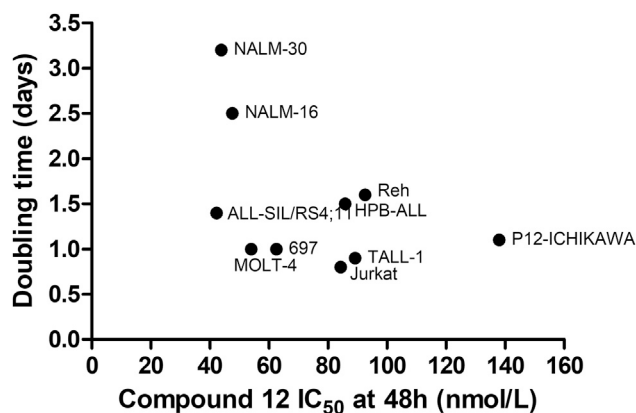
Figure 3. Cell Proliferation and Sensitivity to Compound 12 Do Not Correlate

Eleven ALL cell lines of precursor B cell ALL (Reh, RS4;11, 697, NALM-16, NALM-30) and T cell ALL (Jurkat, ALL-SIL, HPB-ALL, TALL-1, P12-ICHIKAWA, MOLT-4) were analyzed regarding their doubling time and *in vitro* resistance (IC$_{50}$ value; see Table S1) to compound **12** at 48 h. Pearson's r correlation test resulted in a no significant correlation (p = 0.1821 and R^2 = 0.1885).

To determine the structural basis for the different tubulin-binding affinities by compounds **7**, **12**, and **21**, we modeled compounds **7** and **21** into the colchicine-binding site based on the crystal structure of the T$_2$R-TTL-compound **12** complex. These three acylhydrazones only differ in the size of their respective aromatic moiety, which was nicely reflected in the minor rearrangements observed after energy minimization at the end of the βH10-S9 loop and the start of βS9 strand. No perturbations of the βT7 loop or βH7 helix were observed in the models. To accommodate the bromine or methyl moieties of compounds **7** and **21**, respectively, the βH10-S9 loop and the start of βS9 strand shifted slightly away from the colchicine site (Figure S7). Moreover, the 3,4,5-trimethoxy-acylhydrazone moieties minimally moved deeper into the binding pocket by maintaining all binding interactions found in the structure of compound **12**. Finally, the individual changes from a naphthalene to a bromobenzene or a toluene moiety in compounds **7** and **21** only caused a minimal conformational change in the αT5 loop. These observations suggest that both compounds lacking the naphthalene moiety form more favorable interactions with the site, which agrees with their higher binding affinities.

Weight Loss Caused by Acylhydrazones 7, 12, and 21

We have previously shown that compound **12** is at least three orders of magnitude more toxic to leukemia cells than to normal proliferating lymphocytes. In a single-dose acute toxicity study, compound **12** was safe even at the maximum orally administered dose tested (1,000 mg/kg) (Salum et al., 2015). This time, we evaluated all three compounds in repeated dose and dose-escalating toxicity tests, which included also vincristine and colchicine for comparisons. Mice receiving intraperitoneal (i.p.) injections of N-acylhydrazones at a dose of 1 or 10 mg/kg/day, for 2 weeks, showed no weight loss (Figure 6A). Similar results were seen in the treatment with 0.15 mg/kg of vincristine or colchicine. However, mice treated with 1.5 mg/kg of vincristine or colchicine died after 3 to 5 days (Figure 6A), confirming the narrow therapeutic indexes of these drugs.

In the dose-escalating experiment mice receiving daily escalating doses of vincristine and colchicine showed abrupt weight loss followed death at a dose of 38.4 mg/kg. Increasing doses of N-acylhydrazones, on the other hand, were better tolerated. Compound **21** was the most toxic of the three N-acylhydrazones tested. It caused weight loss and death at a dose of 256 mg/kg. Mice receiving compound **7** or **12** did not show significant weight loss or any other clinical sign or behavioral alteration suggestive of intoxication, even at 256 mg/kg (Figure 6B).

In Vivo Anti-leukemia Effects of Compound 12

We have previously shown that compound **12** is able to inhibit the progression of patient-derived B cell precursor ALL cells in immunocompromised mice at a weekly i.p. dose of 1 mg/kg (Salum et al., 2015). Here we preliminarily evaluated different compound **12** treatment schemes on the survival of mice
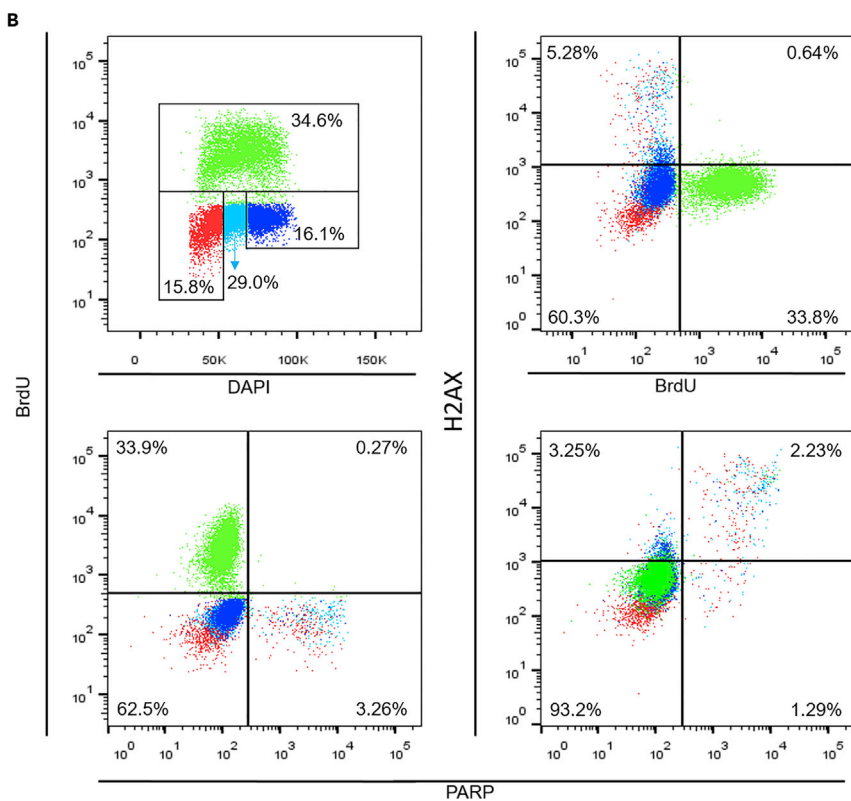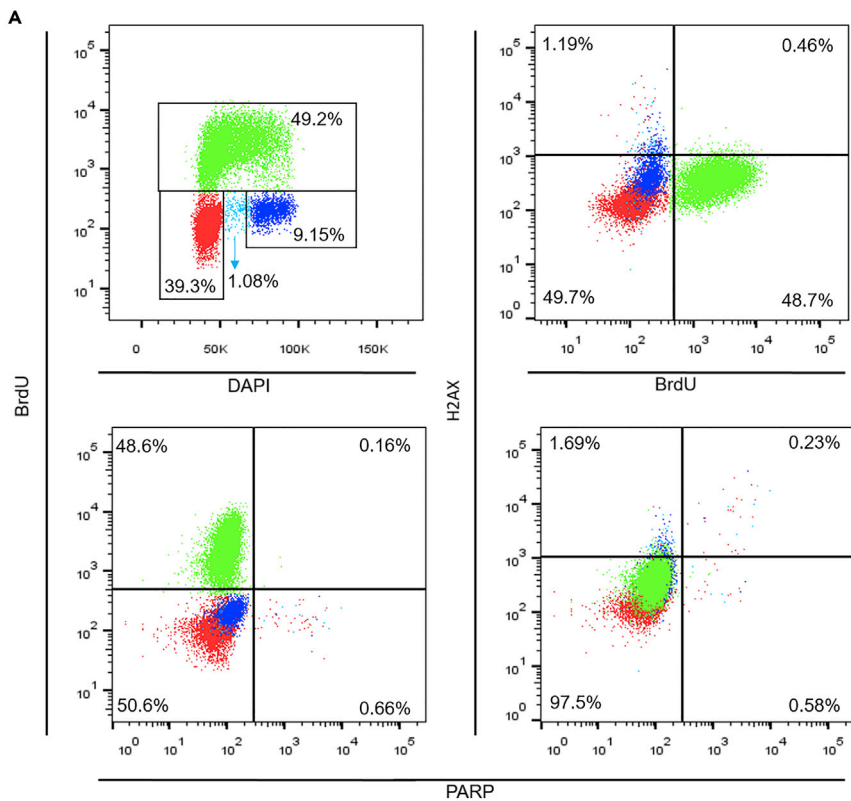
Figure 4. Multiparametric Flow Cytometry Analysis of Cell Cycle, Apoptosis, and DNA Damage in RS4;11 Cells Treated with Compound 12

(A and B) Cells were treated with (A) DMSO (vehicle) 45 nM or (B) compound **12** (IC$_{50}$ dose) for 18 h followed by labeling with 10 μM BrdU for 45 min. The cells were then harvested and analyzed by immunofluorescent staining and multicolor flow cytometric analysis using the BD FACSVerse Flow Cytometer. BrdU-positive cells are color-gated green, whereas BrdU-negative cells at G1 phase, between G1 and G2 phase, and G2 phase of the cell cycle are colored red, light blue, and dark blue, respectively.

transplanted with the RS4;11 ALL cell line. Animals were treated for 4 weeks with DMSO (control); compound **12** at 1 mg/kg, once a week, i.p.; compound **12** at 0.5 mg/kg, thrice a week, every other day, i.p.; or compound **12** at 50 mg/kg, twice a week, orally. As shown in Figure 8, the dose of 1 mg/kg i.p. once a week was not sufficient to prevent leukemia progression or improve survival of mice engrafted with the RS4;11 leukemia cell line. On the other hand, compound **12** at a lower dose of 0.5 mg/kg, i.p., but given thrice a week, had a profound impact on slowing the leukemia progression (Figure 7A) and as a consequence on increasing animal survival (Figure 7B). Apparently, exposure of compound **12** to leukemia cells for a longer time may be advantageous. Oral administration of compound **12** was the second best treatment, however, at the expense of a much higher cumulative dose (100 mg/kg/week). These results suggest that compound **12** has low oral bioavailability.

To validate the use of compound **12** against MDR cells *in vivo*, we use the pre-B cell ALL NALM6 or its MDR counterpart, N6/ADR, which is characterized by P-glycoprotein overexpression (Treichel and Olken, 1992). As expected, compound **12** showed similar IC$_{50}$ values against both NALM6 and N6/ADR, which was not the case for vincristine (Figure S8). Building on the better therapeutic profile of compound **12**, mice were treated with 10 mg/kg, i.p., every day, whereas vincristine was administrated i.p. once a week at a concentration of 0.15 mg/kg (Szymanska et al., 2012). Both vincristine and compound **12** prolonged the overall survival of mice transplanted with NALM6, with vincristine being slightly more efficient than compound **12** (Figure 8A). However, only compound **12** was able to prolong the survival of mice transplanted with N6/ADR (Figure 8B), corroborating with our hypothesis that compound **12** is more efficient than vincristine against MDR leukemia.

DISCUSSION

Vincristine is one of the backbone drugs of ALL treatment. It is a microtubule inhibitor whose major disadvantages are related to its limited bioavailability and high toxicity. Here, we report on three acylhydrazone derivatives with microtubule-depolymerizing activities, which bind to the colchicine-binding site of tubulin, distinctive from the vinca- and taxane-binding sites of the vinca alkaloids and taxanes currently used in clinics.

As most other colchicine-binding site agents, and in contrast to vincristine and vinblastine, compounds **7,12**, and **21** were demonstrated to be active against multidrug resistance (MDR) cells. Only the colchicine-resistant mouse 3T3 embryonic fibroblastoid cell line NIH-MDR-G185 showed a modest resistance to the acylhydrazone compounds; however, it was lower than the resistance observed to colchicine, vinblastine, and vincristine. Of note, the NIH-MDR-G185 cell line was obtained through ectopic expression of the MRD1 gene (Cardarelli et al., 1995), so the levels of P-glycoprotein expression may be much higher than the levels observed in the patient-derived MDR cells. The ability to kill MDR cells may be important in the context of relapsed ALL. Although overexpression of membrane-associated ABC transporter was not associated to vincristine resistance at diagnosis (Holleman et al., 2004), relapsed ALL was shown to express increased levels of multidrug resistance genes, including P-glycoprotein, lung resistance-related protein, and multidrug resistance-associated protein when compared with diagnostic samples (Dhooge et al., 2002; Plasschaert et al., 2005; Terci Valera et al., 2004; van den Heuvel-Eibrink et al., 2000).

Among the three compounds tested, compound **12** is the one with the most favorable cytotoxic activity (Table 1; Salum et al., 2015). Intriguingly, here we show that the tubulin-binding affinity of **12** is not superior but slightly lower than that of compound **7** and 10 times lower than that of compound **21** in the MTC displacement assay. Compound **7** showed a significantly lower cellular uptake than **12**, therefore explaining its lower cellular activity and suggesting that the bromobenzene moiety present in compound **7** has the lowest ability of crossing the cellular membrane compared with the toluene and naphthalene moieties

	Normal Morphology	Micronuclei	p Value[a]	
			Compared with Colchicine	Compared with Vincristine
Vehicle (DMSO)	199	1	<0.0001	<0.0001
Colchicine IC_{50}	174	26	–	<0.0001
Vincristine IC_{50}	99	101	<0.0001	–
12 IC_{50}	163	37	0.1695	<0.0001
12 IC_{90}	131	69	<0.0001	0.0017

Table 2. Micronuclei Formation Induced by Colchicine, Vincristine, and Compound 12
[a]Fisher's exact test. Colchicine IC_{50} = 13.5nM; vincristine IC_{50} = 1.1nM; compound **12** IC_{50} = 81.4nM; IC_{90} = 126.2nM.

present in compounds **21** and **12**, respectively. On the other hand, the cellular uptake of **21** was even better than that of **12**. As compounds **12** and **21** share the same mode of action on tubulin (see below), how can the better cytotoxic activity of **12** be explained, considering that **21** showed higher tubulin-binding affinity and cellular uptake? α-tubulin and β-tubulin are encoded by multigene families, whose members may hold differences in the amino acid composition of their colchicine-binding pocket. Compounds **12** and **21** may have different affinities with each type of tubulin isotype (Kumbhar et al., 2016; Santoshi and Naik, 2014). Leukemia cells express a mixture of different α- and β-tubulin isotypes (data not shown), which is probably not matched by the calf brain tubulin composition used in the MTC displacement assay. Thus the *in vitro* tubulin binding was not a perfect surrogate for the leukemia tubulin binding. Besides, the possibility exists that the higher cellular uptake of **21** is due to off-target or unspecific cellular binding.

Concomitant analysis of cell cycle, DNA damage, and apoptosis revealed that compound **12** promoted DNA damage and apoptosis not only in G2/M but also in G1. Death in G1 probably occurred after unequal division of cells previously arrested in G2/M. Although unequal division could lead to secondary tumors, we found micronuclei formation by compound **12** to be lower than that by vincristine, even at the dose of IC_{90}. Cells in S-phase were not sensitive to compound **12**, which agrees with the fact that no correlation was found between the proliferating index and compound **12**'s IC_{50} values on a series of ALL cell lines.

The crystal structure of the tubulin-compound **12** complex confirmed the binding of compound **12** to the colchicine-binding site of tubulin, which is located between the α- and β-tubulin subunits and shaped by residues of loop T5 of α-tubulin and strands S8, S9, and S10, loop T7, and helices H7 and H8 of β-tubulin (Ravelli et al., 2004). Free tubulin assumes a "curved" conformation. For tubulin to polymerize into micro-tubules this curved conformation has to undergo a conformational change to reach the "straight" structural form of tubulin. During this conformational change, the βT7 loop moves into the colchicine-binding site; however, in the presence of a ligand, the βT7 loop is sterically hindered to assume the straight conformation. As a consequence, tubulin is locked in its curved conformation and becomes assembly incompetent (Prota et al., 2014; Ravelli et al., 2004). Our structural analyses suggest that such a mechanism is indeed also valid for compound **12**. One peculiarity of compound **12** is that it forms only a single hydrogen bond with tubulin, involving the nitrogen of the acylhydrazone linker of compound **12** and the backbone of α-tubulin (residue αThr179). Other colchicine-binding site inhibitors so far characterized were shown to make at least two hydrogen bonds, one of which is always with β-tubulin (Bueno et al., 2018; Gaspari et al., 2017; McNamara et al., 2015; Prota et al., 2014; Wang et al., 2016; Zhou et al., 2016).

Energy-minimized models of both compounds **7** and **21** bound to the colchicine site revealed the same mechanism of action, with no perturbations of the βT7 loop or βH7 helix. Three very small differences were seen: (1) the 3,4,5-trimethoxy-acylhydrazone moiety of **7** and **21** move minimally deeper into the binding pocket; (2) the βH10-S9 loop and the start of βS9 strand shift slightly away from the colchicine-binding site to accommodate the bromine or methyl moieties of compounds **7** and **21**, respectively; and (3) a minimal conformational change in the αT5 loop was recorded. No additional interactions of compounds **7** and **21** with tubulin were observed. These observations suggested that the higher affinities of both compounds **7** and **21** when compared with **12** do not derive from the formation of additional interactions, but rather from the formation of more favorable interactions in the absence of the large naphthalene moiety, which
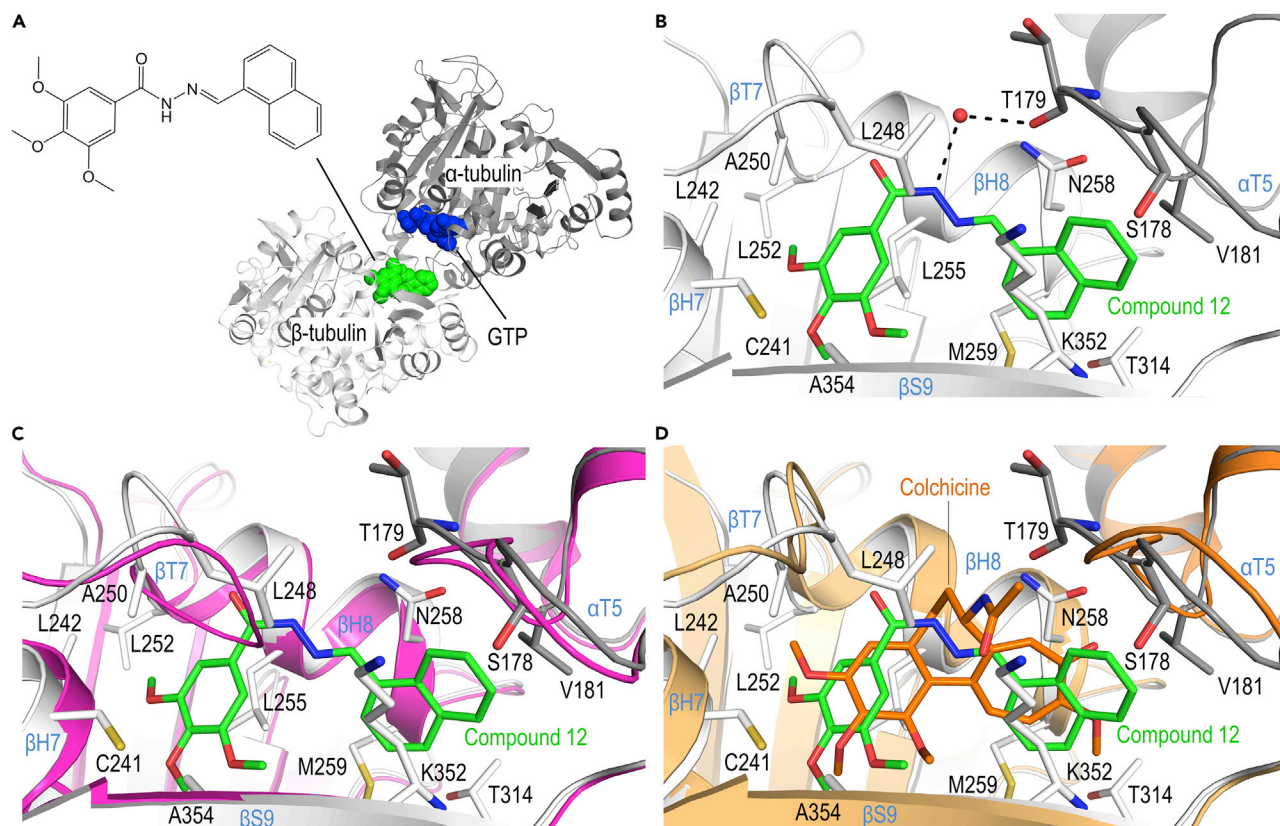
Figure 5. X-Ray Analysis of the T₂R-TTL-Compound 12 Complex

(A) Chemical structure of compound **12** and overall view of the α/β-tubulin heterodimer-compound **12** complex structure. Compound **12** (green spheres) binds at the interface between α-tubulin (dark gray ribbon) and β-tubulin (light gray ribbon) in close proximity to the GTP (blue spheres)-binding site. See also Figure S6 and Table S2.

(B) Close-up view of compound **12** (green sticks) and the surrounding binding pocket formed by α- and β-tubulin using the same color code as in (A). Carbon atoms are depicted in gray for tubulin and green for compound **12**; nitrogen and oxygen atoms are colored in blue and red, respectively. Interacting residues are shown as sticks and are labeled; residues βTyr202, βAla316, βIle318, and βIle378 are omitted for clarity. Secondary structural elements of tubulin are labeled in light blue.

(C) Same view and color code of the tubulin-compound **12** complex as in (B) with the apo T₂R-TTL structure (purple; PDB: 4IHJ) superimposed.

(D) Same view and color code of the tubulin-compound **12** complex as in (B) with the structure of tubulin-colchicine (orange; PDB: 4O2B) superimposed.

occupies a partially hydrophobic pocket in the crystal structure of compound **12**. The modeling data further suggest that the difference in affinity between compounds **7** and **21** likely derives from the differing van der Waals radii of their bromine and methyl moieties, respectively.

An attractive feature of these molecules is that they can be administered in higher doses than vincristine or colchicine. As previously shown (Salum et al., 2015), we here confirm one of these compounds' (compound **12**) strong anti-leukemia activity as a single agent. Our exploratory *in vivo* toxicity test, measuring mice weight loss, revealed that significantly higher doses of *N*-acylhydrazones can be administrated daily to mice when compared with vincristine and colchicine, with no weight loss or clinical sign of toxicity. Compound **21**, however, was lethal at the highest dose tested in the escalating dose study. Whether this increased toxicity is related to its higher neuronal (calf brain tubulin) tubulin-binding affinity or higher cellular uptake remains to be investigated.

Remarkably, compound **12** prolonged the overall survival of mice transplanted with the RS4;11 ALL cell line when given at a dose of only 0.5 mg/kg thrice a week; this dose given thrice a week was shown to be better than 1 mg/kg given once a week. In addition, despite low oral bioavailability, compound **12** was shown to be effective against leukemia when administered by gavage. Pharmacokinetic studies are warranted to improve the treatment schedule. Importantly, we validated the use of compound **12**
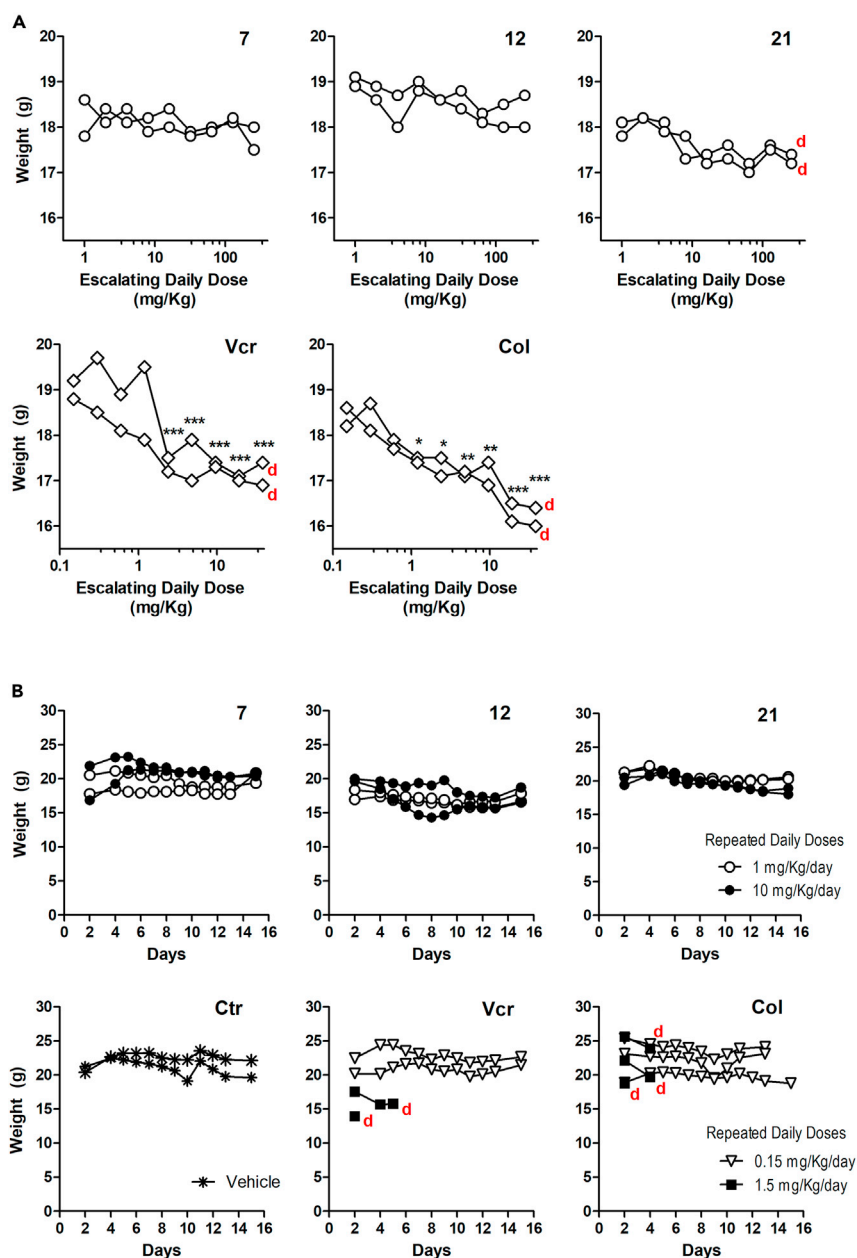
Figure 6. Weight Loss of C57BL/6 Mice Treated with Compounds 7, 12, 21, Vincristine, and Colchicine

(A) Weight loss of C57BL/6 mice treated with escalating daily doses of N-acylhydrazones, vincristine, and colchicine. Groups of two animals received daily i.p. injections of drugs at increasing doses of vincristine, colchicine, compound **7**, compound **12**, or compound **21**. The doses of vincristine and colchicine were 0.15, 0.3, 0.6, 1.2, 2.4, 4.8, 9.6, 19.2, and 38.4 mg/kg. The doses of **7**, **12**, and **21** were 1, 2, 4, 8, 16, 32, 64, 128, and 256 mg/kg.

(B) Weight loss of C57BL/6 mice treated with repeated daily doses of *N*-acylhydrazones, vincristine, and colchicine. Groups of two animals received daily i.p. injections of drugs at two different dosages, during 13 consecutive days. In control (Ctr), animals were injected with vehicle (2% DMSO, 10% Tween 20, 10% glycerol in PBS); d indicates that mouse was dead on the next day. Dots are representative of a single animal. Data were analyzed by two-way ANOVA followed by Bonferroni's post-test for comparison of follow-up weights with the first weight for the corresponding animal (*$p < 0.05$; **$p < 0.01$; ***$p < 0.001$).

for the treatment of animals transplanted with a multidrug-resistant ALL cell line, although the increased survival in this case was shorter than in mice transplanted with the RS4;11 cells, even when higher doses of compound **12** were used (10 mg/kg every day). This probably reflects the higher
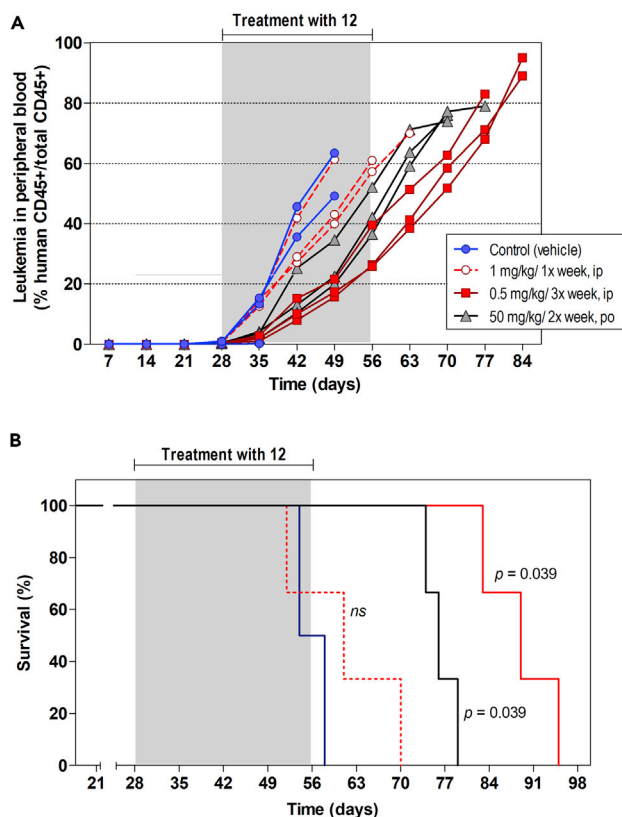
Figure 7. Anti-leukemia Effect of Compound 12 at Different Dose and Administration Routes

NOD/SCID mice were transplanted with RS4;11 ALL cells. After engraftment (>0.5% leukemia cells in peripheral blood mononuclear cells), animals were randomly distributed into groups (n = 3) and treated for 4 weeks with vehicle or the indicated schemes of compound **12**.

(A) Leukemia progression as estimated by the percentage of leukemia cells in peripheral blood after engraftment. Note that leukemia burden was measured every 7 days. Thus, the last measurement of leukemia in the peripheral blood does not correspond to leukemia burden at death.

(B) Kaplan-Meyer survival curves of mice following the indicated schemes of compound **12** administration. Curves were compared by the log rank test. For curves' legend see (A). The indicated p values are for the comparison with the curve of the control group.

aggressiveness of NALM6/N6/ADR, and in any case, vincristine showed no efficacy against MDR cells compared with compound **12**.

In conclusion, we describe new promising colchicine-binding site tubulin inhibitors for the treatment of ALL, featuring a favorable therapeutic index and activity against multidrug-resistant cells. In addition, we provide a structural basis to understand how *N*-acylhydrazones destabilize microtubules, leading to cell death.

Limitations of the Study

Although this study provided information regarding the cellular uptake of compounds **7**, **12**, and **21**, subsequent studies are necessary to investigate the differential metabolization of these compounds by the cell, in particular compound **12**, whose cellular concentration appeared to decrease at the longer time points. This investigation can help design alternative compounds with increased half-life. In addition, in this study we characterized the DNA damage and pro-apoptotic effects of **12** on cells at the different phases of the cell cycle. Besides the expected effects of treatment (cells arrested in G2 and increased numbers of apoptotic sub-G1 cells), we found a sub-population of cells having DNA content in between G1 and G2, which we named "sub-G2" and interpreted as being cells that underwent unequal division of their chromosomes. Cytogenetic analysis by fluorescence *in situ* hybridization of chromosomes would
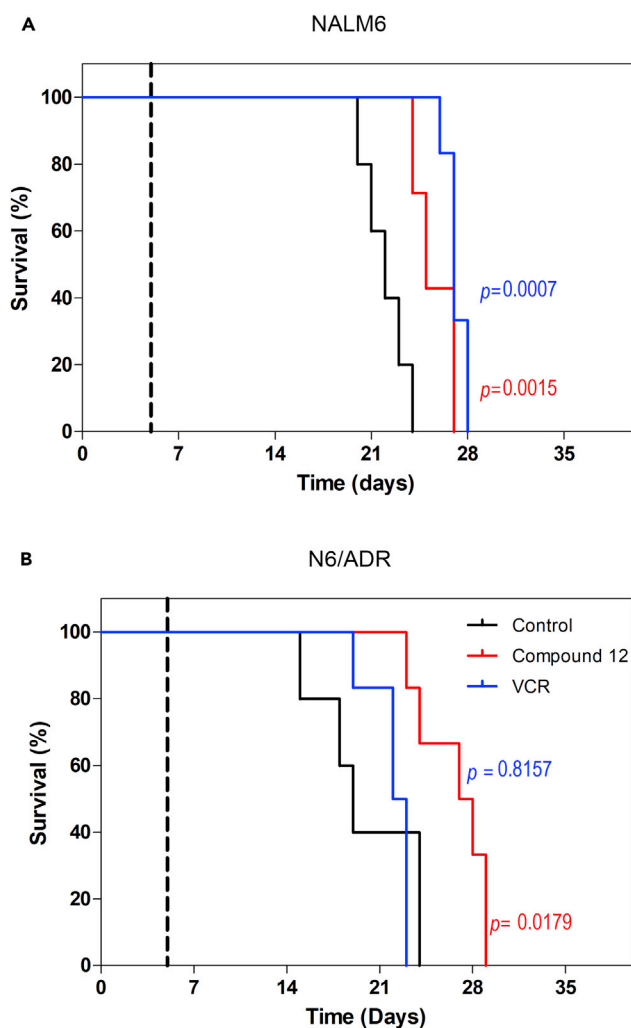
Figure 8. Compound 12 Prolonged Survival of Mice Transplanted with Multidrug-Resistant ALL

(A and B) Kaplan-Meyer survival curves of mice transplanted with (A) NALM6 or the (B) multidrug-resistant N6/ADR ALL cell lines, following treatment with compound **12** (10 mg/kg, i.p., every day), vincristine (0.15 mg/kg, i.p., weekly), or vehicle. Treatment started on the fifth day after transplantation (dashed vertical line). Curves were compared by the log rank test. The indicated p values are for comparison with the curve of the control group. See also Figure S8.

be advisable to validate this finding. Regarding the *in vivo* experiments, it would be interesting to investigate the effect of compound **12** against patient-derived ALL cells with multidrug-resistant phenotype. Last, we noticed increased weight loss of animals receiving compound **12** orally, suggesting either harm by the gavage process or gastrointestinal toxicity at a dose of 50 mg/kg twice a week.

METHODS

All methods can be found in the accompanying Transparent Methods supplemental file.

DATA AND CODE AVAILABILITY

Atomic coordinates and structure factors for the T_2RT-TTL-compound 12 complex have been deposited in the RCSB Protein Data Bank (PDB) under accession number 6F7C.

SUPPLEMENTAL INFORMATION

Supplemental Information can be found online at https://doi.org/10.1016/j.isci.2019.10.003.

AUTHOR CONTRIBUTIONS

N.M.C. performed the majority of the experiments, contributed to the analyses and interpretation of the results, and drafted the manuscript. T.M. performed the crystal structure work and wrote the manuscript. A.B.A.L. performed the in vivo anti-leukemia experiment. R.R.C. supervised the project and contributed to the interpretation of the results. P.P.Z. performed the in vivo toxicity experiment. D.L.-A. contributed to the standardization and interpretation of biochemical results. I.B. contributed to the standardization and analyses of immunofluorescence assay. C.S. and S.D. supervised the in vivo assays with NALM6 and N6/ADR cell lines. D.S. performed mass spectrometry analyzes. R.A.Y. designed and provided the compounds used in the present work. A.E.P. and M.O.S. supervised the crystal structure work and critically reviewed the manuscript. J.F.D. supervised the biochemical work, contributed to the interpretation of the results, and critically reviewed the manuscript. J.A.Y. was responsible for the conception and design of study. He supervised the entire project and wrote the manuscript.

DECLARATION OF INTERESTS

Compounds **7**, **12**, and **21** are patented under WO 2013/075199 A1.

REFERENCES

Antúnez-Mojica, M., Rodríguez-Salarichs, J., Redondo-Horcajo, M., León, A., Barasoain, I., Canales, Á., Cañada, F.J., Jiménez-Barbero, J., Alvarez, L., and Díaz, J.F. (2016). Structural and biochemical characterization of the interaction of tubulin with potent natural analogues of podophyllotoxin. J. Nat. Prod. *79*, 2113–2121.

Bueno, O., Estévez Gallego, J., Martins, S., Prota, A.E., Gago, F., Gómez-Sanjuan, A., Camarasa, M.J., Barasoain, I., Steinmetz, M.O., Díaz, J.F., et al. (2018). High-affinity ligands of the colchicine domain in tubulin based on a structure-guided design. Sci. Rep. *8*, 4242.

Cardarelli, C.O., Aksentijevich, I., Pastan, I., and Gottesman, M.M. (1995). Differential effects of P-glycoprotein inhibitors on NIH3T3 cells transfected with wild-type (G185) or mutant (V185) multidrug transporters. Cancer Res. *55*, 1086–1091.

Dhooge, C., De Moerloose, B., Laureys, G., Ferster, A., De Bacquer, D., Philippe, J., Leroy, J., and Benoit, Y. (2002). Expression of the multidrug transporter P-glycoprotein is highly correlated with clinical outcome in childhood acute lymphoblastic leukemia: results of a long-term prospective study. Leuk. Lymphoma *43*, 309–314.

El-Awady, R., Saleh, E., Hashim, A., Soliman, N., Dallah, A., Elrasheed, A., and Elakraa, G. (2017). The role of eukaryotic and prokaryotic ABC transporter family in failure of chemotherapy. Front. Pharmacol. *7*, 1–15.

Field, J.J., Kanakkanthara, A., and Miller, J.H. (2015). Microtubule-targeting agents are clinically successful due to both mitotic and interphase impairment of microtubule function. Bioorg. Med. Chem. *22*, 5050–5059.

Fitzgerald, T.J. (1976). Molecular features of colchicine associated with antimitotic activity and inhibition of tubulin polymerization. Biochem. Pharmacol. *25*, 1383–1387.

Gaspari, R., Prota, A.E., Bargsten, K., Cavalli, A., and Steinmetz, M.O. (2017). Structural basis of cis- and trans-combretastatin binding to tubulin. Chem *2*, 102–113.

van den Heuvel-Eibrink, M.M., Sonneveld, P., and Pieters, R. (2000). The prognostic significance of membrane transport-associated multidrug resistance (MDR) proteins in leukemia. Int. J. Clin. Pharmacol. Ther. *38*, 94–110.

Holleman, A., Cheok, M.H., den Boer, M.L., Yang, W., Veerman, A.J.P., Kazemier, K.M., Pei, D., Cheng, C., Pui, C.-H., Relling, M.V., et al. (2004). Gene-expression patterns in drug-resistant acute lymphoblastic leukemia cells and response to treatment. N. Engl. J. Med. *351*, 533–542.

Jordan, M.A., Thrower, D., and Wilson, L. (1992). Effects of vinblastine, podophyllotoxin and nocodazole on mitotic spindles. Implications for the role of microtubule dynamics in mitosis. J. Cell Sci. *102* (Pt 3), 401–416.

Kaaijk, P., Kaspers, G.J.L., van Wering, E.R., Broekema, G.J., Loonen, A.H., Hählen, K., Schmiegelow, K., Janka-Schaub, G.E., Henze, G., Creutzig, U., and Veerman, A.J.P. (2003). Cell proliferation is related to in vitro drug resistance in childhood acute leukaemia. Br. J. Cancer *88*, 775–781.

Kumbhar, B.V., Borogaon, A., Panda, D., and Kunwar, A. (2016). Exploring the origin of differential binding affinities of human tubulin isotypes αβII, αβIII and αβIV for DAMA-colchicine using homology modelling, molecular docking and molecular dynamics simulations. PLoS One *11* (5), e0156048.

Liu, Y.-M., Chen, H.-L., Lee, H.-Y., and Liou, J.-P. (2014). Tubulin inhibitors: a patent review. Expert Opin. Ther. Pat. *24*, 69–88.

McNamara, D.E., Senese, S., Yeates, T.O., and Torres, J.Z. (2015). Structures of potent anticancer compounds bound to tubulin. Protein Sci. *24*, 1164–1172.

Oskarsson, T., Söderhäll, S., Arvidson, J., Forestier, E., Montgomery, S., Bottai, M., Lausen, B., Carlsen, N., Hellebostad, M., Lähteenmäki, P., et al. (2015). Relapsed childhood acute lymphoblastic leukemia in the Nordic countries: prognostic factors, treatment and outcome. Haematologica *101*, 68–76.

Plasschaert, S.L.A., de Bont, E.S.J.M., Boezen, M., vander Kolk, D.M., Daenen, S.M.J.G., Faber, K.N., Kamps, W.A., de Vries, E.G.E., and Vellenga, E. (2005). Expression of multidrug resistance-associated proteins predicts prognosis in childhood and adult acute lymphoblastic leukemia. Clin. Cancer Res. *11*, 8661–8668.

Prota, A.E., Bargsten, K., Zurwerra, D., Field, J.J., Diaz, J.F., Altmann, K.-H., and Steinmetz, M.O. (2013a). Molecular mechanism of action of microtubule-stabilizing anticancer agents. Science *339*, 587–590.

Prota, A.E., Magiera, M.M., Kuijpers, M., Bargsten, K., Frey, D., Wieser, M., Jaussi, R., Hoogenraad, C.C., Kammerer, R.A., Janke, C., and Steinmetz, M.O. (2013b). Structural basis of tubulin tyrosination by tubulin tyrosine ligase. J. Cell Biol. *200*, 259–270.

Prota, A.E., Danel, F., Bachmann, F., Bargsten, K., Buey, R.M., Pohlmann, J., Reinelt, S., Lane, H., and Steinmetz, M.O. (2014). The novel microtubule-destabilizing drug BAL27862 binds to the colchicine site of tubulin with distinct effects on microtubule organization. J. Mol. Biol. *426*, 1848–1860.

Soosay Raj, T.A., Smith, A.M., and Moore, A.S. (2013). Vincristine sulfate liposomal injection for acute lymphoblastic leukemia. Int. J. Nanomed. *8*, 4361–4369.

Ravelli, R.B.G., Gigant, B., Curmi, P.A., Jourdain, I., Lachkar, S., Sobel, A., and Knossow, M. (2004). Insight into tubulin regulation from a complex with colchicine and a stathmin-like domain. Nature *428*, 198–202.

Roy, A., Cargill, A., Love, S., Moorman, A.V., Stoneham, S., Lim, A., Darbyshire, P.J., Lancaster, D., Hann, I., Eden, T., and Saha, V. (2005). Outcome after first relapse in childhood acute lymphoblastic leukaemia - lessons from the United Kingdom R2 trial. Br. J. Haematol. *130*, 67–75.

Salum, L.B., Mascarello, A., Canevarolo, R.R., Altei, W.F., Laranjeira, A.B.A., Neuenfeldt, P.D., Stumpf, T.R., Chiaradia-Delatorre, L.D., Vollmer, L.L., Daghestani, H.N., et al. (2015). N-(1'-naphthyl)-3,4,5-trimethoxybenzohydrazide as microtubule destabilizer: synthesis, cytotoxicity, inhibition of cell migration and in vivo activity against acute lymphoblastic leukemia. Eur. J. Med. Chem. *96*, 504–518.

Santoshi, S., and Naik, P.K. (2014). Molecular insight of isotypes specific β-tubulin interaction of tubulin heterodimer with noscapinoids. J. Comput. Aid. Mol. Des. *28*, 751–763.

Shah, N.N., Merchant, M.S., Cole, D.E., Jayaprakash, N., Bernstein, D., Delbrook, C., Richards, K., Widemann, B.C., and Wayne, A.S. (2016). Vincristine sulfate liposomes injection (VSLI, marqibo(R)): results from a phase I study in children, adolescents, and young adults with refractory solid tumors or leukemias. Pediatr. Blood Cancer *63*, 997–1005.

Steinherz, P.G., Gaynon, P.S., Breneman, J.C., Cherlow, J.M., Grossman, N.J., Kersey, J.H., Johnstone, H.S., Sather, H.N., Trigg, M.E., Chappell, R., et al. (1996). Cytoreduction and prognosis in acute lymphoblastic leukemia–the importance of early marrow response: report from the Childrens Cancer Group. J. Clin. Oncol. *14*, 389–398.

Stock, W., Johnson, J.L., Stone, R.M., Kolitz, J.E., Powell, B.L., Wetzler, M., Westervelt, P., Marcucci, G., DeAngelo, D.J., Vardiman, J.W., et al. (2013). Dose intensification of daunorubicin and cytarabine during treatment of adult acute lymphoblastic leukemia: results of Cancer and Leukemia Group B Study 19802. Cancer *119*, 90–98.

Szymanska, B., Wilczynska-Kalak, U., Kang, M.H., Liem, N.L.M., Carol, H., Boehm, I., Groepper, D., Reynolds, C.P., Stewart, C.F., and Lock, R.B. (2012). Pharmacokinetic modeling of an induction regimen for in vivo combined testing of novel drugs against pediatric acute lymphoblastic leukemia xenografts. PLoS One *7*, e33894.

Terci Valera, E., Scrideli, C.A., Gomes de Paula Queiroz, R., Ortelli Mori, B.M., and Gonzaga Tone, L. (2004). Multiple drug resistance protein (MDR-1), multidrug resistance-related protein (MRP) and lung resistance protein (LRP) gene expression in childhood acute lymphoblastic leukemia. Sao Paulo Med. J. *122*, 166–171.

Treichel, R.S., and Olken, S. (1992). The relationship between multi-drug resistance and resistance to natural-killer-cell and lymphokine-activated killer-cell lysis in human leukemic cell lines. Int. J. Cancer *50*, 305–310.

Wang, Y., Zhang, H., Gigant, B., Yu, Y., Wu, Y., Chen, X., Lai, Q., Yang, Z., Chen, Q., and Wang, J. (2016). Structures of a diverse set of colchicine binding site inhibitors in complex with tubulin provide a rationale for drug discovery. FEBS J. *283*, 102–111.

Wood, K.W., Cornwell, W.D., and Jackson, J.R. (2001). Past and future of the mitotic spindle as an oncology target. Curr. Opin. Pharmacol. *1*, 370–377.

Zhou, P., Liu, Y., Zhou, L., Zhu, K., Feng, K., Zhang, H., Liang, Y., Jiang, H., Luo, C., Liu, M., and Wang, Y. (2016). Potent antitumor activities and structure basis of the chiral β-lactam bridged analogue of combretastatin A-4 binding to tubulin. J. Med. Chem. *59*, 10329–10334.

Supplemental Information

Structural Basis of Colchicine-Site targeting

Acylhydrazones active against Multidrug-Resistant

Acute Lymphoblastic Leukemia

Nathália Moreno Cury, Tobias Mühlethaler, Angelo Brunelli Albertoni Laranjeira, Rafael Renatino Canevarolo, Priscila Pini Zenatti, Daniel Lucena-Agell, Isabel Barasoain, Chunhua Song, Dongxiao Sun, Sinisa Dovat, Rosendo Augusto Yunes, Andrea Enrico Prota, Michel Olivier Steinmetz, José Fernando Díaz, and José Andrés Yunes

SUPPLEMENTAL DATA
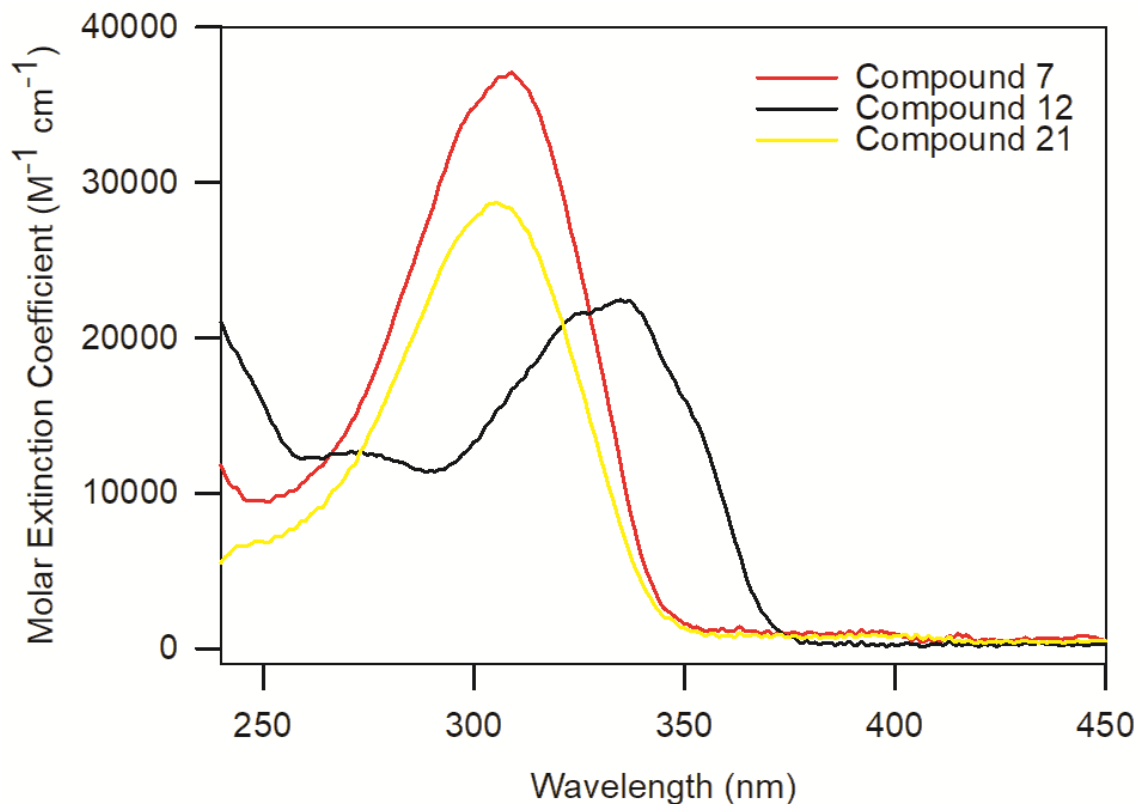
Supplemental Figure S1. UV absorvance spectrum of compounds 7, 12 and 21 at 10 µM, Related to Figure 1A. Compounds were dissolved at a concentration of 5mM in DMSO, and then diluted to 10µM in 10mM Sodium Phosphate. Their UV absorbance spectra were measured in a Thermo Scientific EVOLUTION 201 UV spectrophotometer using blanks with the appropriate concentration of DMSO.
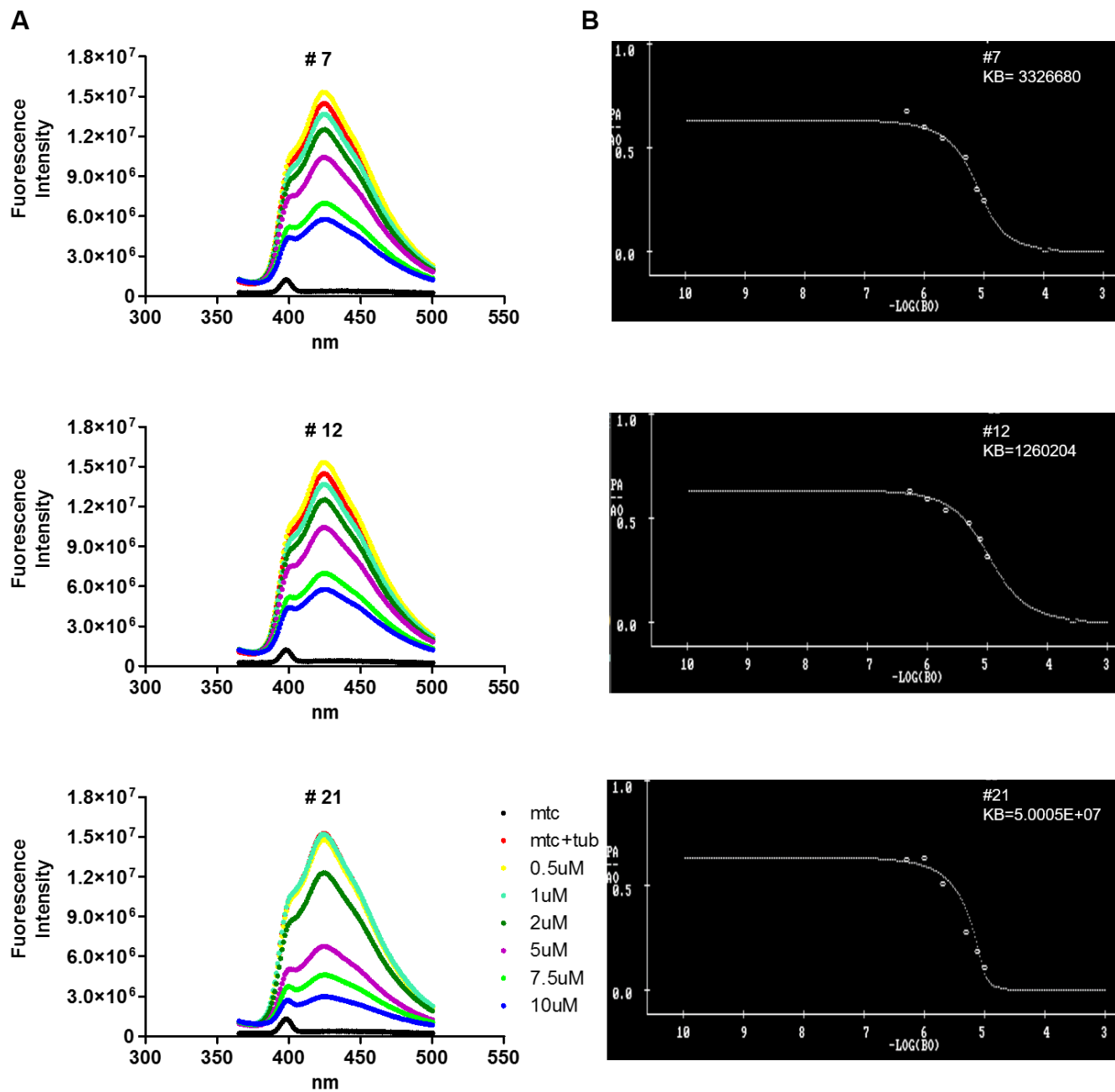
Supplemental Figure S2. Tubulin binding constants for compounds 7, 12, and 21 calculated based on MTC displacement curves, Related to Figure 1B. (**A**) Fluorescence emission spectra of MTC [2-methoxy-5-(2,3,4-trimethoxyphenyl)-2,4,6-cycloheptatrien-1-one] and tubulin in the presence of different concentrations (0.5 to 10 μM) of compound **7**, **12** or **21**. Bottom line is the fluorescence emission spectrum of MTC alone. Each curve represent the mean of three independent experiments. (**B**) Binding constant curves and values calculated by using the DosBox 0.73 software.
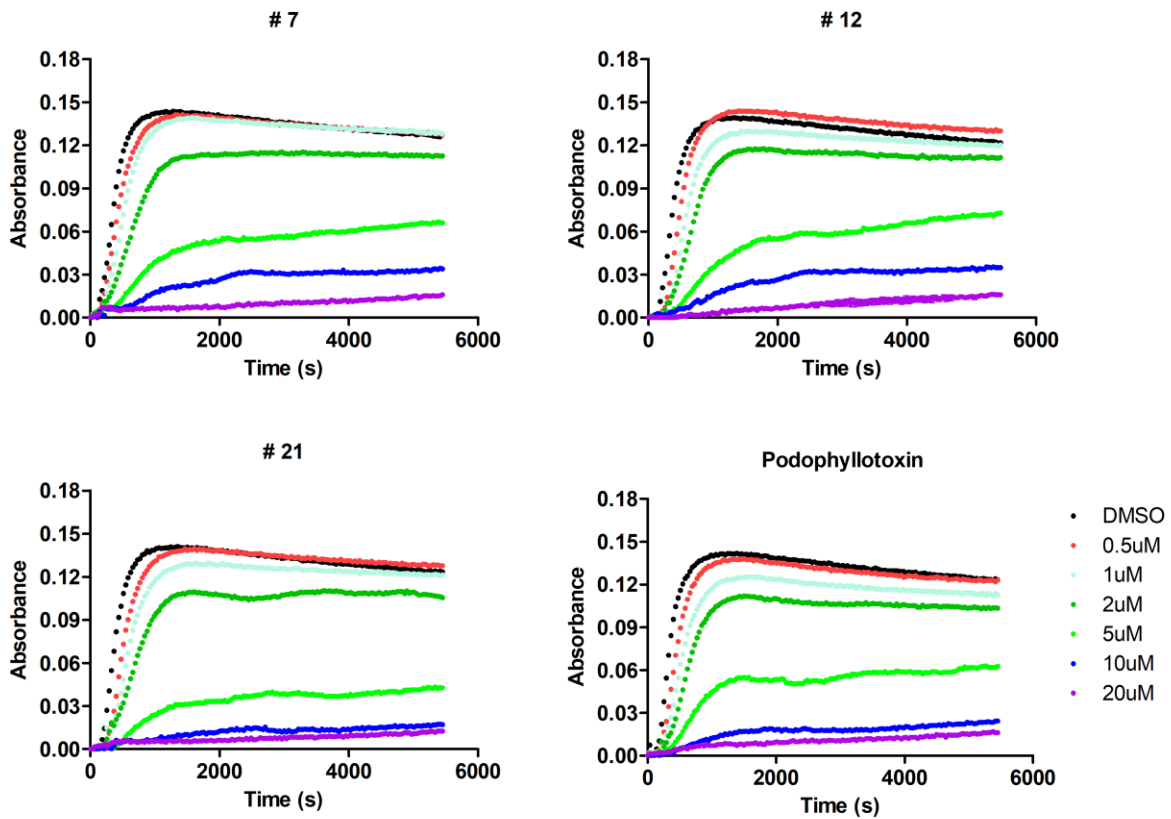
Supplemental Figure S3. In vitro tubulin assembly inhibition by compounds 7, 12, 21, and podophyllotoxin, evaluated by turbidity measurment at a wavelength of 350 nm and 37 °C, Related to Figure 1C. Each curve represent the mean of three independent experiments. Absorbance spectra of 25 μM tubulin in glycerol-assembling buffer, GAB (3.4 M glycerol, 10 mM sodium phosphate, 1 mM EGTA, 1 mM GTP, pH 6.5), in the presence of different concentrations (0.5 to 20 μM) of the ligand studied or 3% of DMSO (vehicle) was monitored along time by turbidity using a Varioskan Flash multimode microplate reader (Thermo Scientific) at a wavelength of 350 nm and 37°C.
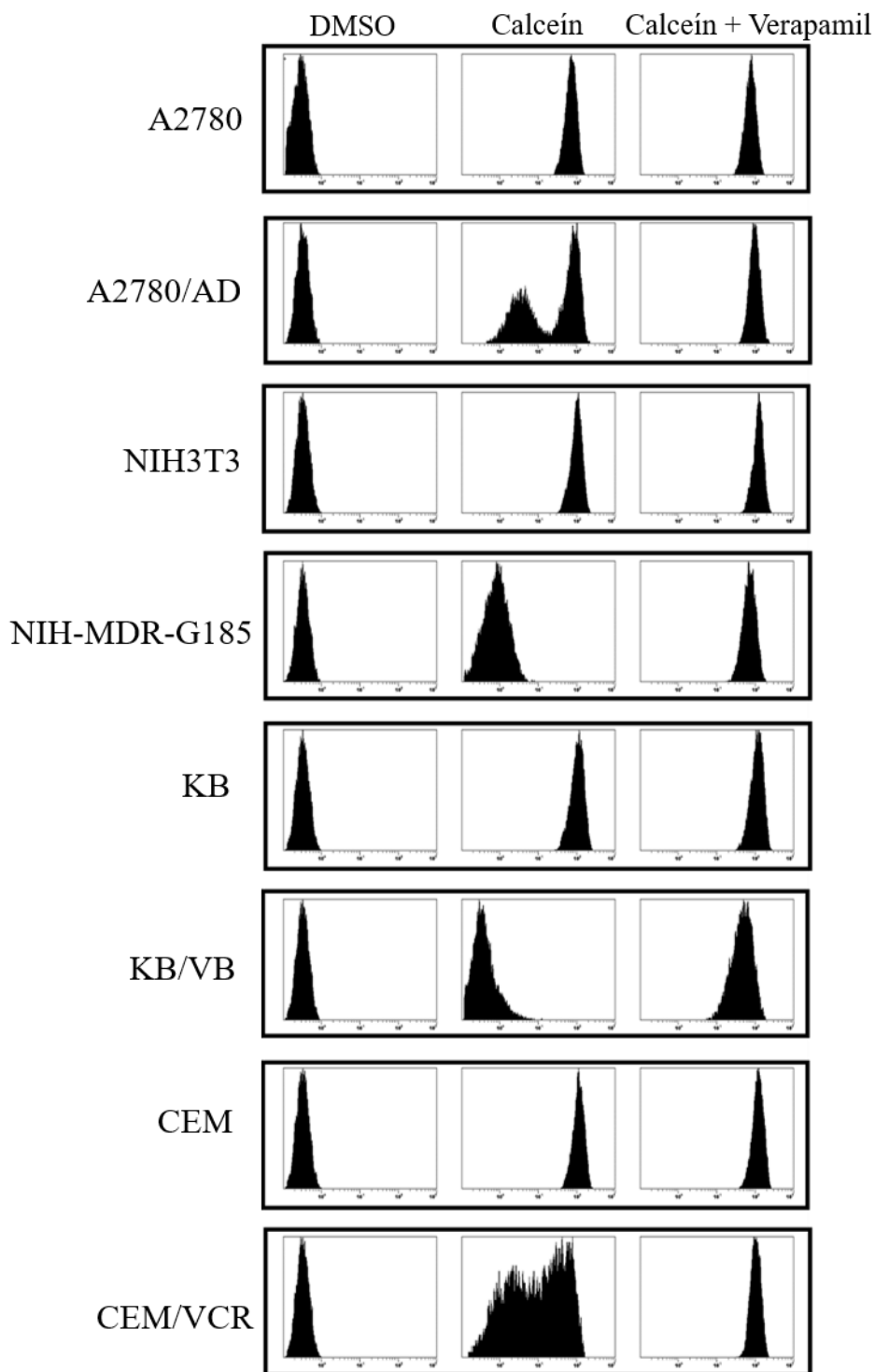
Supplemental Figure S4: Resistant cell lines expressing the Multiple Drug Resistance Phenotype, Related to Table 1. The four pairs of cells used in the cell growth inhibition assay, represented by a sensitive and a resistant cell line, were treated with DMSO, Calceín or Calceín + Verapamil (a P-glycoprotein inhibitor) for 30 minutes and analyzed by flow cytometry. The calceín and verapamil doses were 1 uM and 25 uM respectively.
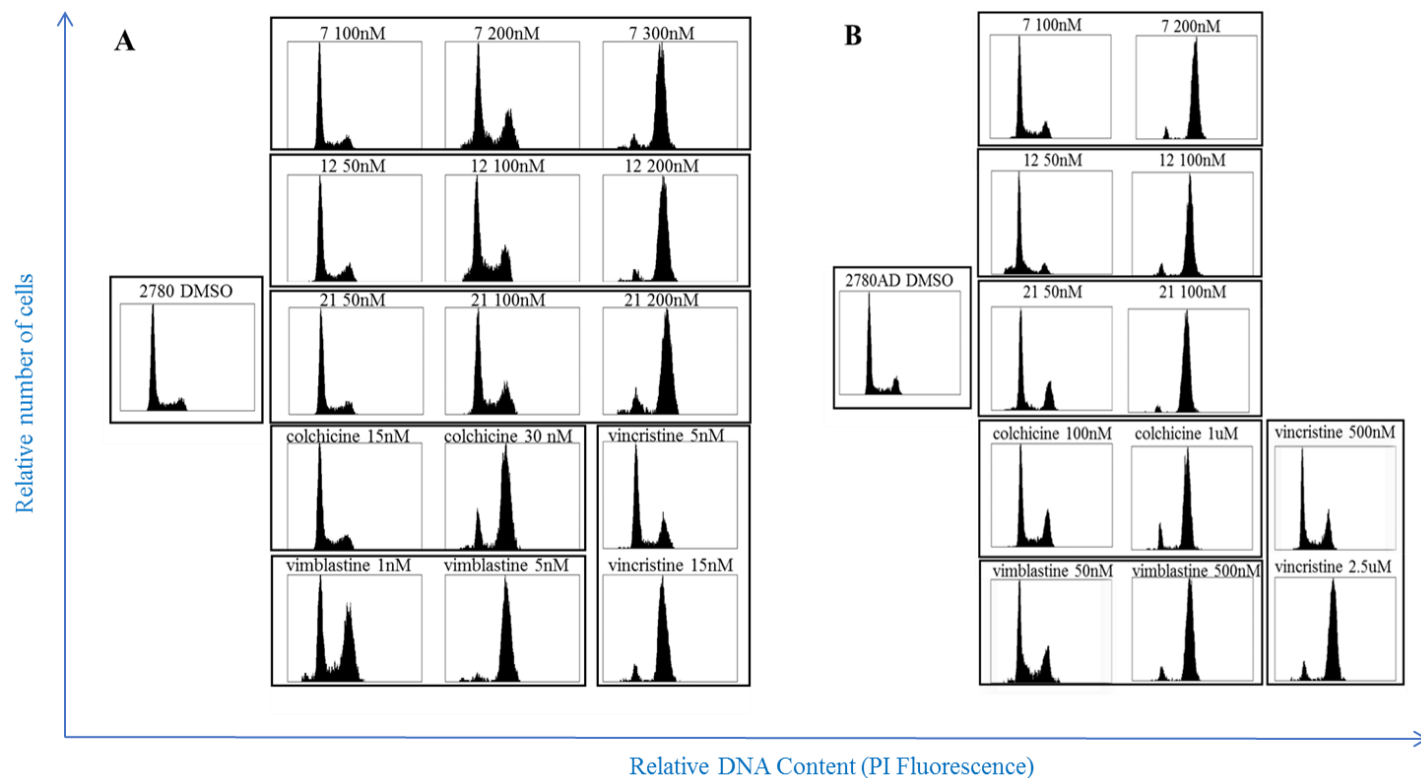
Supplemental Figure S5. Compounds 7, 12 and 21 induce cell cycle arrest in G$_2$/M, Related to Table 1. Cell cycle histograms of (**A**) A2780 (**B**) A2780/AD. Both cells were treated with DMSO (negative control), compounds **7**, **12**, **21**, colchicine, vimblastine and vincristine. Cells were incubated for 20 h at concentrations ranging from 1 nM to 2.5 μM and submitted to cell cycle analysis with propidium iodide staining and flow citometry analysis. The lower ligand concentration that arrests cells in the G2/M phase was depicted.
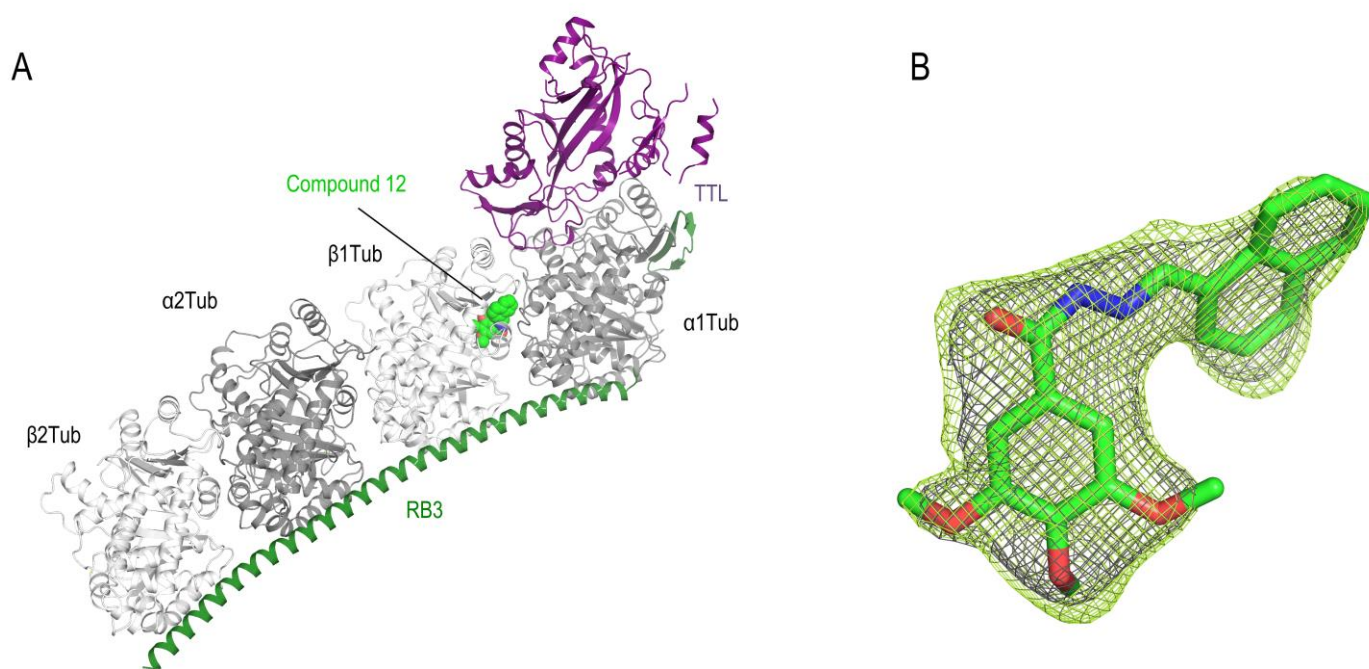
Supplemental Figure S6. Overall view of the T$_2$R-TTL-compound 12 complex structure and electron-density map of compound 12 bound to tubulin in the T$_2$R-TTL complex, Related to Figure 5. (**A**) Overall view of the T$_2$R-TTL-compound **12** complex structure in ribbon representation. The α- and β-tubulin chains are colored in dark and light grey, respectively, TTL is in purple and RB3 is in dark green. The tubulin-bound compound **12** ligand is represented in green spheres. (**B**) Electron-density map of compound **12** bound to tubulin in the T$_2$R-TTL complex. The SigmaA-weighted 2mFo - DFc (dark blue mesh) and mFo - DFc (light green mesh) omit maps are contoured at +0.9σ and +2.5σ, respectively. The map calculations excluded the atoms of the ligand.
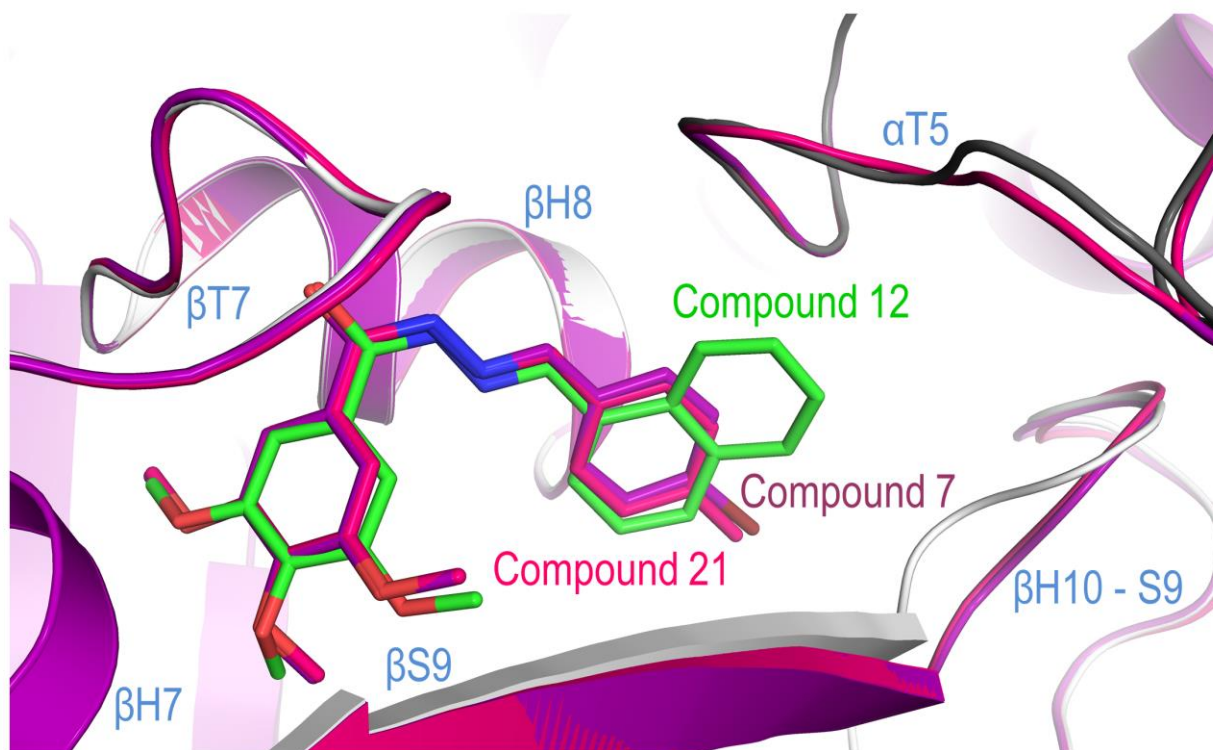
Supplemental Figure S7. Compounds 7 and 21 modeled into the crystal structure of compound 12, Related to Figure 5. Close-up view of compound **12** (green sticks), compound **7** (magenta), and compound **21** (purple) and the surrounding binding pocket formed by α- and β-tubulin represented as ribbons. Ribbons are depicted in grey for tubulin derived from the structure and magenta and purple for the models. Carbon atoms are shown in green for compound **12**, magenta for compound **7** and purple for compound **21**; nitrogen, oxygen and bromine atoms are colored in blue, red and brown, respectively. Secondary structural elements of tubulin are labeled in light blue.

Supplemental Figure S8. Caracterization of sensitive NALM6 and Multidrug-Resistant N6/ADR cell lines, Related to Figure 8. (**A**) NALM6 and N6/ADR cells were treated with Calcein (red histogram) or Calcein + Verapamil (a P-glycoprotein inhibitor; blue histogram) for 30 minutes and analyzed by flow cytometry. The calcein a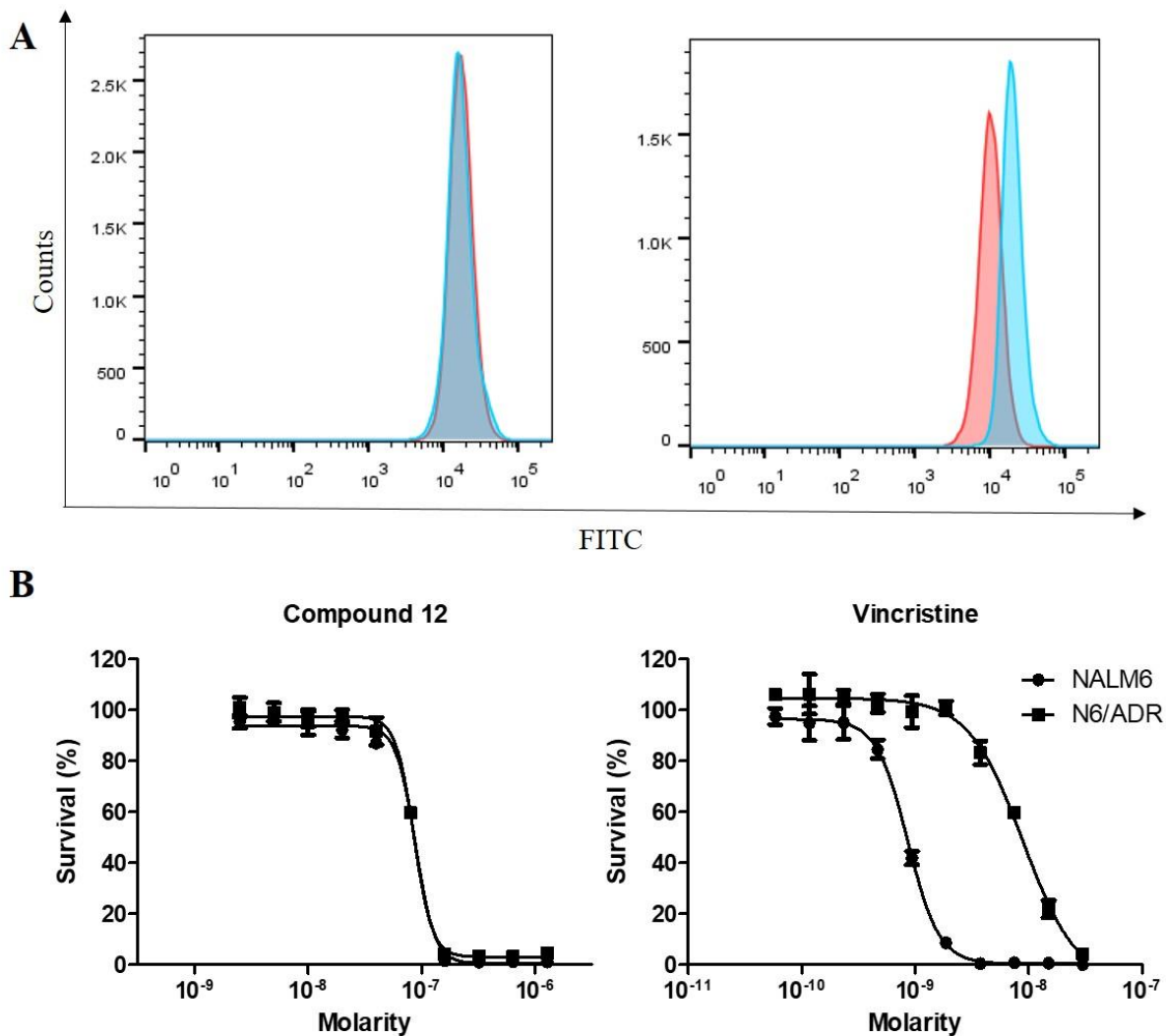nd verapamil doses were 1 uM and 25 uM respectively. (**B**) Survival curves illustrating the cytotoxicity data for compound **12** and vincristine against NALM6 and N6/ADR cell lines after 48 hours of treatment. IC_{50} for compound **12** against NALM6 and N6/ADR were 88.5 nM and 85.8 nM respectively, while IC_{50} for vincristine was 0.87 nM for NALM6 and 9 nM for N6/ADR.

Supplemental Table S1. Proliferation index and Cytotoxicity Data (IC_{50}, nM) for compound 12, against ALL Cell Lines, Related to Figure 3.

ALL cell lines	Doubling time	IC_{50} #**12** (nM)
REH	1.6	92.6
RS4;11	1.4	42.3
697	1.0	62.5
Nalm16	2.5	47.6
Nalm30	3.2	43.9
Jurkat	0.8	84.3
SIL-ALL	1.4	42.3
HPB-ALL	1.5	85.8
TALL-1	0.9	89.2
P12-ICHIKAWA	1.1	138.0
Molt4	1.0	54.0

Supplemental Table S2. X-ray diffraction data collection and refinement statistics of the T$_2$R-TTL-compound 12 complex, Related to Figure 5.

	T$_2$R-TTL-compound 12
Data collection[a]	
Space group	P2$_1$2$_1$2$_1$
Cell dimensions	
a, b, c (Å)	104.5, 157.4, 180.8
Resolution (Å)	59.5 – 2.0 (2.05 – 2.00)
R$_{meas}$ (%)	10.9 (413.1)
R$_{pim}$ (%)	3.3 (118.0)
CC$_{1/2}$[b]	99.9 (25.4)
I/σI	17.8 (0.7)
Completeness (%)	99.8 (98.7)
Redundancy	13.5 (13.2)
Refinement	
Resolution (Å)	59.5 – 2.0
No. unique reflections	199860
R$_{work}$/R$_{free}$ (%)	21.2 / 24.3
Average B-factors (Å^2)	
Complex	63.8
Solvent	55.7
Ligand (chain B)	74.7
Wilson B-factor	45.2
Root mean square deviation from ideality	
Bond length (Å)	0.006
Bond angles (°)	0.773
Ramachandran statistics[c]	
Favored regions (%)	97.46
Allowed regions (%)	2.54
Outliers (%)	0.00

[a] Highest shell statistics are in parentheses. [b] CC1/2= percentage of correlation between intensities from random half-datasets(Karplus and Diederichs, 2012). [c] As defined by MolProbity (Davis et al., 2004).

TRANSPARENT METHODS

3,4,5-trimethoxy-acylhydrazones

Compounds **7**, **12**, and **21** were synthesized as described before (Salum et al., 2015). Identity and purity were confirmed by mass spectrometry and nuclear magnetic resonance. For *in vitro* experiments, compounds were dissolved in dimethyl sulfoxide (DMSO) from Sigma-Aldrich (St. Louis, MO, USA). DMSO concentration in the assay was $\leq 0.5\%$. For animal experiments, compound **7**, **12**, or **21** were dissolved in DMSO at 10 mg/mL. Then, a volume corresponding to 10 mice's injection was mixed with 100 μL of Tween 20 and 880 μL of PBS, incubated at 37ºC for 5 min, and 100 μL were injected per animal. For UV absorbance spectra, the compounds were dissolved at a concentration of 5 mM in DMSO, and then diluted to 10uM in 10 mM sodium phosphate. Their UV absorbance spectra were measured in a Thermo Scientific EVOLUTION 201 UV spectrophotometer using blanks with the appropriate concentration of DMSO.

Cell lines culture and viability assays

We used five pairs of cells and their MDR derivates in this study: 1) The human ovarian cancer cell line A2780 and its MDR derivative, A2780/AD; 2) CCRF-CEM (CEM) and CEM-vincristine-resistant (CEM/VCR (Haber et al., 1989)), which were a generous gift from Professor Maria Kavallaris (Children Cancer Institute, Australia), 3) KB-3-1 (KB) cell line derived from human epidermal carcinoma cells and its MDR mutant derivative KB-V1 resistant to vinblastine (KB/VB) (Shen et al., 1986), 4) NIH3T3 cell line established from NIH Swiss mouse embryo cultures and its MDR NIH-MDR-G185 cell line, that is a clone of NIH3T3 cells transfected with the retroviral vector pHaMDR1/A (wild-type glycine at position 185), resistant to colchicine

(Cardarelli et al., 1995), 5) B-ALL NALM6 cell line and its MDR derivate N6/ADR (ATCC® CRL-3274) also used in an *in vivo* assay. The human non small cell lung carcinoma A-549 cells (ATCC® CCL-185) as well as the adherent cells A2780, A2780/AD, KB, KB/VB, NIH3T3 and NIH-MDR-G185 used in this study were grown in DMEM supplemented with 10% fetal bovine serum, 2 mM L-glutamine, and 100 U/mL penicillin and 100 µg/mL streptomycin (Sigma-Aldrich, Saint Louis, MO, USA). The acute lymphoblastic leukemia cell lines NALM6, N6/ADR, CEM, CEM/VCR, Nalm16, Nalm30, REH, SIL, RS4;11, HPB, 697, Molt4, P12-Ichikawa, Tall-1 and Jurkat were cultured in RPMI-1640 (Cultilab, Campinas, SP, Brazil) supplemented with 10% fetal bovine serum (Cultilab), penicillin 100 IU/mL and 100 µg/mL streptomycin. Cells were maintained in a 5% CO_2-humidified incubator at 37°C. RS4;11 B-cell ALL cell used in the in vivo study was kindly provided by Dr. Sheila A. Shurtleff (St Jude Children's Research Hospital, Memphis, TN).

Cell viability experiments were performed in 96-well micro-titer plates using the MTT reduction assay (0.5mg/ml final concentration, 4 hrs incubation) after 48 h of treatment. The formazan dye formed by the viable cells was dissolved by the addition of acid sodium dodecyl sulfate solution (10% SDS, 0.01 mol/L HCl). Following overnight incubation, absorbance was measured at 570 nm and 620 nm. Percentage of cell survival was calculated in relation to controls. IC_{50} values were calculated from dose-response curves using the GraphPad Prism 5 (GraphPad Software, La Jolla, CA, USA) software.

Immunofluorescence Analysis

A-549 cells were plated (160,000 cells/mL) and cultured overnight in 24-well tissue culture plates containing 12 mm round coverslips. Next, cells were treated with different

concentrations of the drugs or vehicle (DMSO) for 24 h. Cells were permeabilized with 0.5% Triton X100 and fixed with 3.7% formaldehyde, as previously described (de Ines et al., 1994). Then, cells were incubated with the anti-α-Tubulin monoclonal antibody, DM1A (Sigma-Aldrich) for 1 hour and 30 minutes at 37°C , washed twice in PBS and incubated with FITC-conjugated secondary goat anti-mouse polyvalent immunoglobulins antibody (Sigma-Aldrich) for 1 hour at 37°C. The coverslips were washed, and the nuclei of the remaining cells were labeled with 1 μg/mL of Hoechst 33342 for 30 min. Finally, samples were washed, examined and photographed using a Zeiss Axioplan epifluorescence microscope. The images were recorded with a Hamamatsu ORCA-FLASH 4.0 cooled CCD camera.

Tubulin Polymerization Assay

Polymerization of 25 μM calf brain tubulin maintained in glycerol-assembling buffer (3.4 M glycerol, 10 mM sodium phosphate, 1 mM EGTA, 1 mM GTP, pH 6.5), and in the presence of different concentrations of the ligand studied or 3% of DMSO (vehicle) was monitored along time by turbidity using a Varioskan Flash multimode microplate reader (Thermo Scientific) at a wavelength of 350 nm and 37 °C.

Ligand Binding to Tubulin

The effect of different concentrations of compounds **7**, **12** and **21** in the binding of 2-methoxy-5-(2,3,4-trimethoxyphenyl)-2,4,6-cycloheptatrien-1-one (MTC) (Fitzgerald, 1976) to calf brain tubulin was verified as described previously (Andreu et al., 1998; Regina et al., 2007). Briefly, different concentrations (0.5 to 10 μM) of compound **7**, **12** or **21** were added to 10 μM tubulin and 10 μM MTC in 10 mM sodium phosphate, 0.1 mM GTP buffer, pH 7.0. The

incubation of 30 minutes for compounds **7** and **21** and one hour for compound **12**, at room temperature, was followed by measurement of fluorescence emission spectra of MTC in the FluoroMax-2 equipment. Binding constants were calculated using the EQUIGRA 5 software (Díaz and Buey, 2007).

Analysis of cellular uptake by HPLC-MS/MS

Five million CEM (T-ALL) cells were treated with 100 nM of compounds **7**, **12**, or **21**. After 0.5, 6 or 12h. Cells were collected, washed 3x times with cold PBS, pelleted by centrifugation, ressuspended in 350 µL of PBS and sonicated for three cycles of 20 seconds in a Bioruptor equipment (Liege, Belgium). Total protein was measured using the BCA Protein Assay Kit (Thermo Fisher Scientific Waltham, MA) and compounds were quantified by mass spectrometry. Standard solutions at different concentrations were prepared by serial dilutions of each compound in methanol. Compound **21** (95 ng/mL) was used as internal standard for compound **12** analysis, and compound **12** (100 ng/mL) was used as internal standard for compounds **7** and **21** analyses. Calibration standards were prepared by mixing 20 µL of blank cell homogenate, 6 µL of standard solution, 6 µL internal standard and 28 µL of methanol (to precipitate the proteins), to final standard concentrations from 1 ng/mL to 1000 ng/mL. Homogenates (20 µL) from drug treated cell samples were mixed with 6 µL of internal standard and 34 µL methanol. Samples were vortexed, followed by centrifugation at 4°C for 10 min at 8765 *g*. The supernatants were analyzed using an ABSciex 4000 Q Trap mass spectrometry coupled with a Waters Acquity UPLC separation system. A 1.7 µm Acquity UPLC BEH C18 analytical columm (2.1 x 100 mm, Waters, Ireland) was used and the gradient elution was conducted using a flow rate of 0.3 mL/min with the following conditions: Initiate in 10% mobile phase B

(acetonitrile) and 90% solvent A (0.1 % formic acid in water), a linear gradient to 100% mobile phase B in 2 minutes, and keep the 100% mobile phase B for 2 minutes to flush the column. The autosampler was kept at 4°C, and the column temperature was maintained at 35°C. The ABSciex 4000 Q Trap mass spectrometer was equipped with an electrospray ionization probe operated in positive mode. The decluster potential (DP) for compound **12**, **21** and **7** was 77 V, 83 V and 78 V respectively; the entrance potential (EP) was 9 V, the collision energy (CE) for compound **12**, **21** and **7** was 27.6 V, 27.6 V and 31.8 V respectively; the collision cell exit potential (CXP) for compound **12**, **21** and **7** was 14 V, 15.5 V and 14.6 V respectively. The curtain gas (CUR) was 10 L/h, the collision gas (CAD) was 12 h/L. The ionSpray voltage was 5500 V, the temperature was 550°C, the ion source gas 1 was 60 h/L and the ion source gas 2 was 50 h/L. The multiple reaction monitoring mode (MRM) was used to analyze and quantify the 3 compounds, with the transitions of m/z 365 > 195 for compound **12**, 329 > 195 for compound **21** and 393 > 195 for compound **7**. All peaks were integrated and quantified by ABSciex Multiquan 3.1 software. The standard curves were constructed by plotting the ratio of the peak area of the analyte to the peak area of internal standard versus analyte concentration. The amount of compounds obtained by mass spectrometry analysis was normalized by the amount of protein from the same sample.

Cell Cycle Analysis

For cell cycle analysis, 180,000 cells in 1 mL were incubated with different concentrations of the drugs for 20 h, then fixed in 70% ethanol, washed with PBS, and incubated at 37°C for 15 min in 1 mL PI Buffer (0.1% Triton X-100, 0.2 mg/mL RNAse, and 20 μg/mL propidium iodide, in PBS). Ten thousand events were analyzed in a Coulter Epics XL flow

cytometer. RS4;11 analysis of cell cycle and apoptosis was performed following the Apoptosis, DNA Damage and Cell Proliferation Kit protocol from BD Pharmingen™.

Micronuclei formation

$1{,}5 \times 10^6$ Jurkat T-ALL cells in 5 mL were incubated with vehicle (DMSO), colchicine (IC_{50} dose= 13.5 nM), vincristine (IC_{50} dose= 1.1 nM) and compound **12** at the dose of IC_{50} (81.4 nM) and IC_{90} (126.2 nM) for 24 h. Cells were harvested followed by Wright staining procedure for 3 minutes. A total of 200 cells were counted for each treatment using the Olympus BX51 microscope.

In vivo weight loss using escalating and repeating doses of compounds 7, 12 and 21.

C57BL/6 mice were acquired from the animal facility of the State University of Campinas. Animals were housed in individually ventilated cages, at 22 ± 1 ºC, under a 12-h light/12-h dark cycle, with food and tap water ad libitum. The numbers of animals, study design, and treatment of animals were reviewed, and approved by the Ethics Committee in Animal Experimentation of the State University of Campinas and registered under Protocol #3624-1. For the dose-escalating study, ten 7- to 8-weeks-old mice were randomly distributed in five groups (compounds **7**, **12**, **21**, vincristine and colchicine) of two animals. Escalating doses of drugs, 2x-fold daily increase, were given intraperitoneally (ip) for 9 consecutive days. For compounds **7**, **12** and **21** the doses used were 1, 2, 4, 8, 16, 32, 64, 128 and 256 mg/kg. For vincristine and colchicine the doses used were 0.15, 0.3, 0.6, 1.2, 2.4, 4.8, 9.6, 19.2, and 38.4 mg/kg. Control mice were administered the same volume of vehicle (2% DMSO in saline). Mice death, weight loss, intake of food and drink were registered during the 9 days.

For the repeated-dose study, twenty-two C57BL/6 mice >10 weeks old were randomly divided in six groups and received daily ip injections of the test compounds for 13 consecutive days. Two different dosages were tested: 1 mg/kg and 10 mg/kg for compounds **7**, **12**, and **21**; 0.15 mg/kg and 1.5 mg/kg for vincristine and colchicine. Control group of animals received vehicle (2% of DMSO, 10% of Tween, 10% of glycerol and 78% of PBS). The location of the ip injection was alternating between lower left and lower right abdominal quadrants. Mice death and weight were registered until day fifteen.

In vivo **drug treatment of ALL xenografts mice transplanted with a human ALL**

Animal experiment using RS4;11 cell line was approved by the Ethics Committee in Animal Experimentation of the State University of Campinas and registered under Protocol #3624-1. Ten million RS4;11 cells were washed with PBS and injected in unconditioned NOD/SCID (NOD.CB17-Prkdcscid/J) mice (The Jackson Laboratory, Bar Harbor, ME) via the tail vein. Animals were monitored every 7 days for leukemia engraftment.(Lock et al., 2002) Briefly, blood was collected by retro-orbital bleeding into EDTA containing tubes, mononuclear cells were isolated by ficoll centrifugation and labeled with anti-human CD45-PE (clone HI30, BD Pharmingen,San Diego, CA or EXBIO, Prague, Czech Republic) and anti-mouse CD45-FITC (clone 30F-11, BD Pharmingen) antibodies. The presence and quantity of leukemia cells was evaluated by flow cytometry in a FACSCanto II equipment (Becton Dickinson, Franklin Lakes, NJ). When human CD45(+) cells reached 0.5% of total CD45 peripheral blood cells in half of the animals, they were randomly distributed among the different treatment groups: placebo (saline solution), compound **12** (1 mg/kg, 1x per week, intraperitoneally), compound **12** (0.5 mg/kg, 3x per week, every other day, intraperitoneally) or compound **12** (50 mg/kg, 2x per

week, oral). Compound **12** was poorly dissolved when given at 50 mg/kg. Treatment lasted four weeks only. Every week, before the administration of saline or compound **12**, weight was recorded and blood was collected to measure the percentage of leukemic cells (hCD45+ cells) by flow cytometry, as already described. Overall survival was measured from the date of inoculation to animal death.

The animal experiment using NALM6 and N6/ADR cells were conducted under protocol number #46695 approved by the Institutional Animal Care and Use Committee at Penn State Hershey, Hershey, PA. NALM6 and N6/ADR cells ($5x10^4$) were injected via tail vein into 4-6-week-old NRG, NOD-Rag1null IL2rgnull, NOD rag gamma mice (The Jackson Laboratory). Starting five days after cell injection, mice (n=5-6 per group) received vehicle (1% PVP, 4% DMSO, 95% PBS), compound **12** or vincristine daily via intraperitoneal at 10mg/kg/day until their death. Overall survival was measured from the date of inoculation to animal death. After death, animals were checked for splenomegaly to confirm the death from leukemia. When necessary, flow cytometry analysis of spleen cells using anti human CD19 and CD10 antibodies was performed.

Crystallization, data collection and structure determination

Crystals of T2R-TTL were grown as described by Prota et al. (A. E. Prota et al., 2013; Andrea E. Prota et al., 2013). Briefly, the T2R-TTL complex was crystallized by the vapor-diffusion method at 20°C. Crystals grew over night in precipitant solution consisting of 5% PEG 4K, 16% glycerol, 30 mM MgCl2, 30 mM CaCl2, 100 mM MES/Imidazole, pH 6.5. The crystals were soaked for 3 hours at 20°C in reservoir solutions containing 5 mM of compound **12**, 10% PEG 4K and 16% glycerol, followed by a consecutive transfer to reservoir solutions containing

20% glycerol before flash-cooling in liquid nitrogen. Native data were collected at 100K at beamline X06SA of the Swiss Light Source (Paul Scherrer Institut, Villigen, Switzerland). Data were processed and merged with XDS (Kabsch, 2010). The T_2R-TTL-compound **12** structure was determined by the difference Fourier method using the phases of the T_2R-TTL complex (PDB ID 5LXT) in the absence of ligands and solvent molecules as a starting point for refinement. The models were first fitted by several cycles of rigid body refinement followed by simulated annealing and restrained refinement in Phenix (Adams et al., 2010). The resulting models were further improved through iterative model rebuilding in Coot (Emsley and Cowtan, 2004) and refinement in Phenix. The quality of the structures was assessed with MolProbity (Davis et al., 2004). Data collection and refinement statistics are given in Supplemental Table S1. Chains in the T_2R-TTL complex were defined as follows: chain A, α1-tubulin; chain B, β1-tubulin; chain C, α2-tubulin; chain D, β2-tubulin; chain E, RB3; chain F, TTL. Structure visualization, molecular editing and figure preparation were performed with the PyMOL molecular graphics system (The PyMOL Molecular Graphics System, Version 1.8.4.2. Schrödinger, LLC).

Modeling

To rationalize the observed structure/affinity relationship between the studied agents, both compound **7** and **21** were first modeled into the colchicine site using the binding pose of the 3,4,5-trimethoxy-acylhydrazone moiety of compound **12** as a starting point and then minimized by using the MAB all atom force field in Moloc (Gerber and Muller, 1995). To accommodate the ligands, only the αT5- (173-182), the βT7- (245-251) and the βH10-S9-residues (343-352) were relaxed during energy minimization, while all remaining residues were kept fixed.

Statistical analysis

The statistical tests are mentioned in each figure legend. Statistical analyses were performed using the GraphPad Prism 5 (GraphPad Software, La Jolla, CA, USA) software.

Data and Software Availability

The accession number for the T_2RT-TTL-compound **12** complex reported in this paper is PDB: 6F7C.

SUPPLEMENTAL REFERENCES

Adams, P.D., Afonine, P. V., Bunkóczi, G., Chen, V.B., Davis, I.W., Echols, N., Headd, J.J., Hung, L.W., Kapral, G.J., Grosse-Kunstleve, R.W., McCoy, A.J., Moriarty, N.W., Oeffner, R., Read, R.J., Richardson, D.C., Richardson, J.S., Terwilliger, T.C., Zwart, P.H., 2010. PHENIX: A comprehensive Python-based system for macromolecular structure solution. Acta Crystallogr. Sect. D Biol. Crystallogr. 66, 213–221.

Andreu, J.M., Perez-Ramirez, B., Gorbunoff, M.J., Ayala, D., Timasheff, S.N., 1998. Role of the colchicine ring A and its methoxy groups in the binding to tubulin and microtubule inhibition. Biochemistry 37, 8356–8368.

Cardarelli, C.O., Aksentijevich, I., Pastan, I., Gottesman, M.M., 1995. Differential Effects of P-Glycoprotein Inhibitors on NIH3T3 Cells Transfected with Wild-Type (G185) or Mutant (V185) Multidrug Transporters. Cancer Res. 55, 1086–1091.

Davis, I.W., Murray, L.W., Richardson, J.S., Richardson, D.C., 2004. MolProbity: Structure validation and all-atom contact analysis for nucleic acids and their complexes. Nucleic Acids Res. 32.

de Ines, C., Leynadier, D., Barasoain, I., Peyrot, V., Garcia, P., Briand, C., Rener, G.A., Temple, C., 1994. Inhibition of Microtubules and Cell Cycle Arrest by a New l-Deaza-7,8-dihydropteridine Antitumor Drug, CI 980, and by Its Chiral Isomer, NSC 613863. Cancer Res. 54, 75–84.

Díaz, J.F., Buey, R.M., 2007. Characterizing Ligand-Microtubule Binding by Competition Methods. Methods Mol Med. 137, 245-60.

Emsley, P., Cowtan, K., 2004. Coot: Model-building tools for molecular graphics. Acta Crystallogr. Sect. D Biol. Crystallogr. 60, 2126–2132.

Fitzgerald, T.J., 1976. Molecular features of colchicine associated with antimitotic activity and inhibition of tubulin polymerization. Biochem. Pharmacol. 25, 1383–1387.

Gerber, P.R., Muller, K., 1995. MAB, a generally applicable molecular force field for structure modelling in medicinal chemistry. J. Comput. Aided. Mol. Des. 9, 251–268.

Haber, M., Norris, M.D., Kavallaris, M., White, L., Stewart, B.W., Bell, D.R., Davey, R.A., 1989. Atypical Multidrug Resistance in a Therapy-induced Drug-resistant Human Leukemia Cell Line (LALW-2): Resistance to Vinca Alkaloids Independent of P-Glycoprotein. Cancer Res. 49, 5281–5287.

Kabsch, W., 2010. XDS. Acta Crystallogr D Biol Crystallogr 66, 125–132.

Karplus, P.A., Diederichs, K., 2012. Linking crystallographic model and data quality. Science (80-.). 336, 1030–1033.

Lock, R.B., Liem, N., Farnsworth, M.L., Milross, C.G., Xue, C., Tajbakhsh, M., Haber, M., Norris, M.D., Marshall, G.M., Rice, A.M., 2002. The nonobese diabetic/severe combined immunodeficient (NOD/SCID) mouse model of childhood acute lymphoblastic leukemia reveals intrinsic differences in biologic characteristics at diagnosis and relapse. Blood 99, 4100–4108.

Prota, A. E., Bargsten, K., Zurwerra, D., Field, J.J., Diaz, J.F., Altmann, K.-H., Steinmetz, M.O., 2013. Molecular Mechanism of Action of Microtubule-Stabilizing Anticancer Agents. Science (80-.). 339, 587–590.

Prota, A. E., Magiera, M.M., Kuijpers, M., Bargsten, K., Frey, D., Wieser, M., Jaussi, R., Hoogenraad, C.C., Kammerer, R.A., Janke, C., Steinmetz, M.O., 2013. Structural basis of tubulin tyrosination by tubulin tyrosine ligase. J. Cell Biol. 200, 259–270.

La Regina, G., Edler, M.C., Brancale, A., Kandil, S., Coluccia, A., Piscitelli, F., Hamel, E., Martino, G. De, Matesanz, R., Dı, F., Scovassi, A.I., Prosperi, E., Moro, P.A., 2007. Arylthioindole Inhibitors of Tubulin Polymerization . 3 . Biological Evaluation , Structure - Activity Relationships and Molecular Modeling Studies 2865–2874.

Salum, L.B., Mascarello, A., Canevarolo, R.R., Altei, W.F., Laranjeira, A.B.A., Neuenfeldt, P.D., Stumpf, T.R., Chiaradia-Delatorre, L.D., Vollmer, L.L., Daghestani, H.N., De Souza Melo, C.P., Silveira, A.B., Leal, P.C., Frederico, M.J.S., Do Nascimento, L.F., Santos, A.R.S., Andricopulo, A.D., Day, B.W., Yunes, R.A., Vogt, A., Yunes, J.A., Nunes, R.J., 2015. N-(1'-naphthyl)-3,4,5-trimethoxybenzohydrazide as microtubule destabilizer: Synthesis, cytotoxicity, inhibition of cell migration and in vivo activity against acute lymphoblastic leukemia. Eur. J. Med. Chem. 96, 504–518.

Shen, D.W., Cardarelli, C., Hwang, J., Cornwell, M., Richert, N., Ishii, S., Pastan, I., Gottesman, M.M., 1986. Multiple drug-resistant human KB carcinoma cells independently selected for high-level resistance to colchicine, adriamycin, or vinblastine show changes in expression of specific proteins. J. Biol. Chem. 261, 7762–7770.